Physicochem. Probl. Miner. Process., 62(1), 2026, 217430

http://www.journalssystem.com/ppmp

Physicochemical Problems of Mineral Processing

ISSN 1643-1049

Linking mineralogical variability to processing: Strategies for a rare earth carbonatite deposit

Ezgi Akyildiz [1], Camilo M. Silva [1], Stefanie Lode [1,2], Kornel Tobiczyk [1], Przemyslaw B. Kowalczuk [1]

[1] Norwegian University of Science and Technology (NTNU), Department of Geosciences, S.P. Andersens vei 15a, 7031, Trondheim, Norway

[2] The Geological Survey of Norway, Leiv Eirikssons vei 39, 7040 Trondheim, Norway

Corresponding author: ezgi.akyildiz@ntnu.no (Ezgi Akyildiz), pshem.kowalczuk@ntnu.no (Przemyslaw B. Kowalczuk)

Abstract: The global demand for rare earth elements continues to rise, while newly discovered deposits typically exhibit lower ore grades as most high-grade resources have already been exploited. Their extraction is often constrained by complex mineralogy. Economically important rare earth minerals such as bastnäsite and monazite typically occur in fine-grained, heterogeneous assemblages with carbonates and silicates as gangue minerals. Linking mineralogical variability to beneficiation performance enables the identification of suitable concentration techniques, including gravity, magnetic, electrostatic, and froth flotation methods. This study employs a process mineralogical approach to characterize low-, medium-, and high-grade intervals of a rare earth carbonatite drill core containing monazite, parisite, bastnäsite, and synchysite, and to evaluate their implications for mineral processing. Elemental and mineralogical data are investigated to evaluate beneficiation potential and guide flowsheet development. At the current grind size, each sample grade has the potential to achieve acceptable recovery, each exhibiting distinctive characteristics. Low-grade sample may require specific conditions due to the phosphate nature of the main target mineral (monazite). Medium-grade sample may exhibit limited efficiency in magnetic separation due to higher association degree between magnetite and the target minerals and reduced selectivity during flotation due to its higher apatite content. High-grade sample, containing the highest Fe-bearing carbonates, may require the use of tailored reagents to maintain satisfactory separation. The findings emphasize that grade-specific process design, informed by elemental and mineralogical characterization, is essential to maximize rare earth recovery. This integrated approach provides a framework for optimizing beneficiation strategies in complex REE-bearing carbonatite deposits.

Keywords: rare earth minerals, parisite, bastnäsite, monazite, beneficiation, automated mineralogy

1. Introduction

Rare earth elements (REEs) are becoming increasingly essential for clean energy, electronics, defense, and advanced manufacturing, yet their extraction is challenging due to complex mineralogy and variable sample grades. Economically important rare earth minerals (REMs), such as bastnäsite ($(Ce,La,Nd,Y)(CO_3)F$), monazite ($(Nd,La,Ce)PO_4$), and xenotime (YPO_4), typically occur in fine-grained, heterogeneous assemblages with diverse gangue minerals including carbonates and silicates (Balaram, 2019; Drobniak and Mastalerz, 2022). A thorough understanding of the mineralogical characteristics of ore deposits is therefore essential for the design of efficient and selective beneficiation strategies (Jordens et al., 2013; Bradshaw, 2014; Petruk, 2000). Mineral exploration techniques involve identifying minerals and determining the mineralogical characteristics of rocks and sample deposits. The results of such mineralogical studies are often used to predict the locations of sample deposits, the potential for recovering specific minerals or elements, and the behavior of sample during mineral processing (Petruk, 2000). Most sample deposits display substantial variability arising from their geological formation and mineralogical composition, both of which exert a decisive influence on beneficiation performance

DOI: 10.37190/ppmp/217430

(Wang et al. 2020). Process mineralogy provides a framework for quantifying and interpreting this complexity by generating critical data on mineral abundances, liberation characteristics, and mineral associations. These datasets are essential for evaluating sample variability, designing robust and efficient flowsheets, minimizing the need for prolonged bench-scale testing, and serving as diagnostic tools for troubleshooting beneficiation performance (Grammatikopoulos and Downing, 2020; Aasly, 2024). A particularly important dimension of process mineralogy lies in tracking how modal mineralogy, elemental deportment, liberation, and mineral associations vary along the length of a drill core. Such variations can significantly influence processing outcomes by influencing both grade distribution and recovery potential. For example, changes in the proportion of gangue or accessory minerals may reduce flotation selectivity, alter reagent requirements, or even require the incorporation of additional separation stages (Bradshaw, 2014). Methods such as gravity, magnetic, electrostatic separation, and froth flotation target specific mineral properties, but their efficiency depends strongly on mineral associations and liberation characteristics (Drzymala, 2007; Wills and Finch, 2016; Al-Ali et al., 2020). Understanding the mineralogical patterns at an early stage allows for better prediction of metallurgical behavior, improved resource characterization, and ultimately, a more reliable transition from exploration to production (Lotter et al., 2018). The beneficiation of REMs presents significant technological challenges (Jordens et al., 2013). Addressing these challenges requires the application of modern, quantitative analytical techniques that provide not only chemical but also mineralogical and microstructural information. Bulk chemical analyses of samples and processing products using X-ray fluorescence (XRF) and inductively coupled plasma mass spectrometry (ICP-MS) yield elemental concentrations. X-ray diffraction (XRD) enables mineral phase identification, but its reliability decreases markedly when mineral abundances fall below approximately 1 wt.% (Schulz et al., 2019). Moreover, both XRF/ICP-MS and XRD require finely powdered samples and provide no information on particle size, mineral grain size, particle composition, mineral intergrowths, or liberation characteristics. These parameters are, however, critical for understanding and optimizing REEs beneficiation. Consequently, non-destructive, element-sensitive techniques based on scanning electron microscopy (SEM) coupled with energy-dispersive spectroscopy (EDS), incorporating automated backscattered electron (BSE) image analysis – collectively referred to as automated mineralogy – are widely applied (Schulz et al., 2019). Applied mineralogy techniques provide extensive opportunities for characterizing primary resources as well as processing by-products and mine tailings, which typically exhibit complex compositions (Abaka-Wood et al., 2019; Gronen et al., 2019; Buchmann et al., 2020; Guner et al., 2023; Malafeevskiy et al., 2025). In a study conducted on Zr-REE-Nb ore from Khalzan Buregtei, SEM-based automated mineralogy (SEM-AM) was utilized to identify the sample properties for the economic exploitation of the mineralized rocks of this deposit (Gronen et al., 2019). The insights enable efficient pre-concentration of rare-metal ores at coarser particle sizes, thereby reducing the need for energy-intensive comminution. Schulz et al. (2019) aimed to develop and apply a robust, generic classification scheme for REE-bearing minerals in automated SEM-based – mineralogical analysis (MLA) by labelling EDS spectra based on bulk-normalised Si, Ca, F, and P contents, thereby overcoming uncertainties in mineral identification, and to use this approach to quantitatively evaluate mineralogical characteristics and beneficiation performance (liberation, locking, grain size distribution, and grade–recovery behavior) of REEs carbonatite ores (Schulz et al., 2019).

AM has proven to be a key technology for the comprehensive characterization of both primary and secondary raw materials as well as being used as a diagnostic tool (Gu et al., 2014; Bagger et al., 2025). Its ability to deliver quantitative insights into mineralogy, texture, and elemental deportment makes it invaluable for plant optimization, feasibility studies, and process design. Through detailed assessment of mineral associations, liberation, and modal composition, AM supports informed decision-making across the entire mining value chain from resource evaluation to the development and optimization of beneficiation strategies (Gu et al., 2014; Becker 2023).

Most of the previous studies about Fen complex have predominantly focused on the geological background such as origin, mineralization and paragenesis rather than processing-based evaluation (Brøgger, 1921; Andersen, 1984; Kresten and Morogan, 1986; Andersen, 1986; Andersen, 1987; Andersen, 1988; Lie and Østergaard, 2011; Boesche et al., 2016; Elliot et al, 2018; Marien et al., 2018; Dahlgren, 2019; Cagno et al., 2020). There are a few studies focusing on beneficiation of REMs or extraction of REEs from the

sample (Davris et al., 2018; Silva et al., 2023; Gajendra et al., 2025, Akyildiz et al., 2026). In this study, chemical and mineralogical characteristics of low-, medium- and high-grade samples originating from a carbonatite-type rare earth deposit (Fen complex) were analyzed via ICP-MS and SEM-AM analyses. Our work aims to evaluate different beneficiation methods such as gravity, magnetic separation and froth flotation for each grade based on elemental assays, modal mineralogy, mineral liberation at the current grind size and mineral associations. Each sample was investigated separately to capture a broader range of responses and account for potential differences in separation behavior.

2. Materials and methods

2.1. Sample preparation

The different samples namely, low-, medium-, and high-grade were ground to below 150 μm using a high-pressure grinding roll (HPGR) and split into representative subsamples for subsequent characterization and beneficiation tests.

2.2. Chemical analysis

The samples were analyzed via ICP-MS using a PerkinElmer SCIEX-ELAN DRC-II spectrometer featuring axial field technology. Approximately, a 0.4 g of material from each sample was digested in a 65% concentrated HNO_3 solution at 85 °C for 20 hours. TREO, defined as La_2O_3 + CeO_2 + Pr_6O_{11} + Nd_2O_3, were used to report the ICP-MS results, consistent with conventional REEs concentrate reporting practices (Geoscience Australia, 2023; Nkiawete and Wal, 2025). TREO values were calculated using established stoichiometric conversion factors for each oxide (James Cook University, n.d.). (Total REEs (TREE) = La + Ce + Pr + Nd)

2.3. Particle size distribution analysis

The particle size distribution (PSD) of ground sample was measured by Malvern Panalytical Mastersizer 3000. Each sample was measured 3 times, and the average of these measurements was used to determine the particle size distribution.

2.4. Mineralogical analysis

SEM-AM analysis was performed at the Department of Geosciences of NTNU (IGV) . The analyses were acquired using a ZEISS Sigma 300VP field emission SEM equipped with two Bruker X-flash 6|60, 129 eV energy dispersive spectroscopy (EDS) detectors and ZEISS Mineralogic Software v.1.08.02, Mining plug-in. The following microscope settings were used: 8.5 mm working distance (WD), 20kV acceleration voltage, and an aperture of 120 μm. The step size was set to 2 μm due to fine intergrowths of various minerals. For the investigations, grain mounts were prepared as polished blocks of samples mixed with epoxy (Logitech 2 Part Epoxy Resin Type 301) in pucks of 30 mm diameter (Røisi and Aasly, 2018). Mineral associations, indicating which mineral grains share grain boundaries within the particles, are automatically obtained through analysis using ZEISS Mineralogic software, which identifies mineral phases and maps their spatial relationships by calculating the partial perimeter at the contact between mineral phases. This automated analysis provides visual and quantitative data on the bulk mineralogy, mineral associations, element assays, as well as liberation and locking properties. Mineral liberation by partial perimeters were used to assess the liberation degree of minerals. The grains with exposed perimeter more than 90% were classified as 'liberated', between 90% - 30% as 'composites' and with lower than 30% as 'locked'. Mineral association analysis was done for the most abundant mineral subtypes (parisite-Ce, parisite-Ce-La, bastnäsite-Ce-La, monazite-Ce and synchysite-Ce) as well as magnetite, a potential by-product. The detailed elemental criteria used to define the main mineral subtypes and their REEs assays are provided as mineral recipes in Appendix A1.

3. Results

3.1. Chemical analysis

Elemental concentration of the sample grades obtained from ICP-MS analyses are given in Table 1. Ce is the dominant REE in all sample grades, followed by La, Nd, and Pr. The TREO contents of the low-, medium-, and high-grade samples are 0.33, 1.12, and 2.18 wt.%, respectively.

Table 1. Elemental concentration of the sample grades based on ICP-MS analyses

Sample grade	Low	Medium	High
Element	**wt.%**	**wt.%**	**wt.%**
Y	0.00	0.00	0.00
La	0.08	0.31	0.65
Ce	0.14	0.46	1.01
Pr	0.01	0.04	0.07
Nd	0.04	0.13	0.09
Sm	0.01	0.02	0.02
Eu	0.00	0.00	0.00
Gd	0.01	0.02	0.02
Tb	0.00	0.00	0.00
Dy	0.00	0.00	0.00
Ho	<LOD	0.00	0.00
Er	<LOD	0.00	0.00
Tm	<LOD	<LOD	<LOD
Yb	<LOD	0.00	<LOD
Lu	<LOD	<LOD	<LOD
Th	0.02	0.05	0.02
Fe	5.30	5.96	8.06
TREE	0.28	0.94	1.82
TREO	0.33	1.12	2.18

* LOD: Limit of detection

3.2. Particle size distribution

PSD analysis results are presented in Fig. 1. The low- and medium-grade samples exhibited very similar distributions, whereas the high-grade sample displayed slightly coarser particle size with higher Dx (50) and Dx (90) values (40 µm and 107 µm, respectively), indicating a reduced proportion of fine particles compared to the low- and medium-grade samples (Table 2).

Table 2. PSD parameters for the low-, medium-, and high-grade samples after grinding to below 150 µm

Sample grade	Low	Medium	High
Dx (10)	4.2 µm	4.1 µm	5.6 µm
Dx (50)	31.3 µm	29.5 µm	40.3 µm
Dx (90)	95.0 µm	97.1 µm	107.0 µm

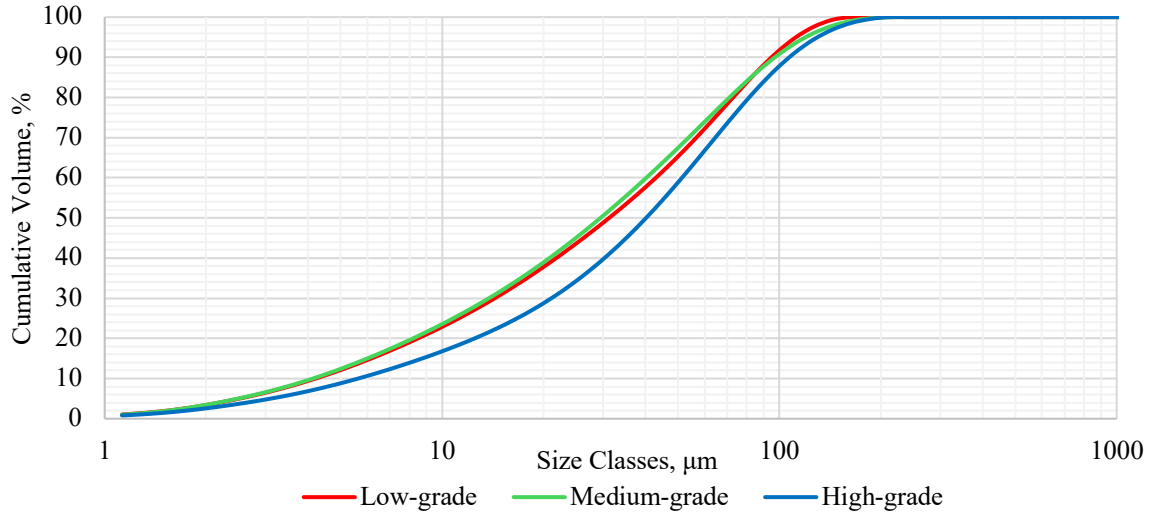

Fig. 1. Particle size distribution of the ground samples

3.3. Mineralogical analysis

3.3.1. Modal mineralogy

Quantitative modal mineralogy (wt.%) of the samples analyzed is presented in Table 3. In the low-grade sample, monazite (0.43 wt.%) and parisite (0.39 wt.%) are the dominant REMs, followed by bastnäsite (0.08 wt.%) and synchysite (0.04 wt.%). Parisite is the main REM in the medium-grade sample (1.49 wt.%), whereas bastnäsite (1.59 wt.%) predominates in the high-grade sample.

Table 3. Quantitative modal mineralogy (wt.%) of the samples analyzed – sorted starting from the main gangue minerals. 'Others' refers to minerals present at <0.1 wt. %

Mineral	**Bulk (wt.%)**		
Sample grade	Low	Medium	High
Parisite	0.39	1.49	1.20
Monazite	0.43	0.90	0.37
Bastnäsite	0.08	0.32	1.59
Synchysite	0.04	0.03	0.04
Ferroan dolomite	33.40	14.03	22.96
Ankerite	31.72	45.42	56.66
Calcite	25.34	25.03	1.45
Apatite	2.37	5.60	1.17
Magnetite	2.12	2.25	3.20
Dolomite	1.22	0.52	1.03
Pyrite	0.77	0.43	1.63
Barite	0.68	1.44	4.95
Chlorite_Fe-Mg	0.53	0.47	1.75
Biotite	0.25	0.04	0.28
Others	0.66	2.03	1.69

Table 4. Chemical formulas and densities of the minerals identified in low-, medium- and high-grade samples – sorted starting from the main REMs and the main gangue minerals (Deer et al., 2013; Jordens et al., 2013; Li et al., 2022; Webmineral, 2025)

Mineral	**Chemical formula**	**Density (g/cm³)**
Parisite	$Ca(Ce,La,Nd)_2(CO_3)_3F_2$	4.20 – 4.50
Monazite	$(Nd,La,Ce)PO_4$	4.98 – 5.43
Bastnäsite	$(Ce,La,Nd,Y)(CO_3)F$	3.90 – 5.20
Synchysite	$Ca(Ce,La,Nd)(CO_3)_2F$	3.90 – 4.14
Ferroan dolomite	$Ca(Mg,Fe)(CO_3)_2$	2.80 – 2.90
Ankerite	$Ca(Fe,Mg,Mn)(CO_3)_2$	2.93 – 3.10
Calcite	$Ca(CO_3)$	2.71
Dolomite	$CaMg(CO_3)_2$	2.84
Apatite	$Ca_5(PO_4)_3(Cl,F,OH)$	3.19
Magnetite	Fe_3O_4	5.15
Pyrite	FeS_2	5.01
Barite	$BaSO_4$	4.48
Chlorite	$(Fe,Mg,Al)_{4\text{-}6}(Si,Al)_4O_{10}(OH,O)_8$	2.60 – 3.30

Fig. 2 shows the total REMs (TREM= parisite + bastnäsite + monazite + synchysite) content of different sample grades. Low-, medium- and high-grade samples contain 0.9, 2.7 and 3.2 wt.% of TREM, respectively.

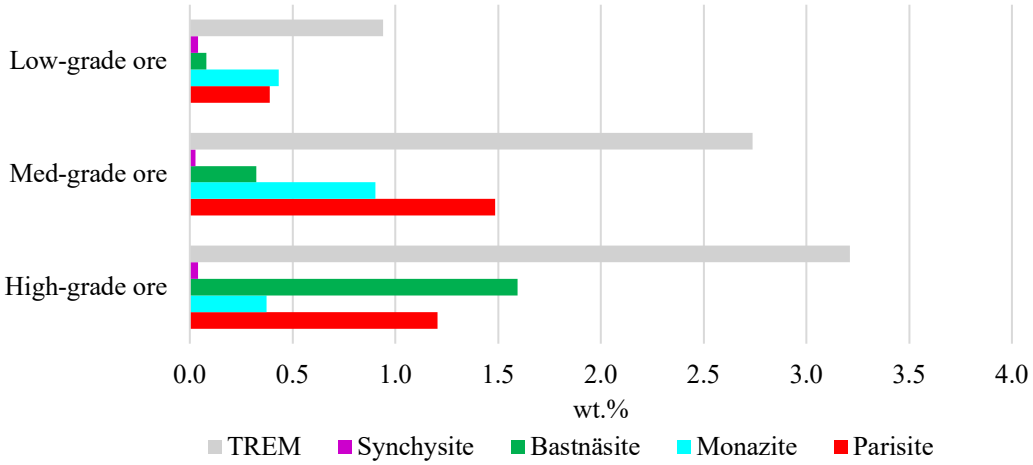

Fig. 2. REMs and TREM contents of different sample grades as determined by automated mineralogy

The relative REMs content of the low-, medium- and high-grade sample is presented in Fig. 3. The low-grade sample contains the highest relative proportion of monazite (46%) compared with the other sample grades (33% in the medium- and 12% in the high-grade sample). In the medium-grade sample, parisite constitutes 54% of the TREM, while bastnäsite accounts for 12%. In the high-grade sample, bastnäsite and parisite accounts for 50% and 38% of the TREM, respectively. The relative modal abundance of synchysite in low-, medium-, and high-grade samples are 4%, 1 and 1%, respectively.

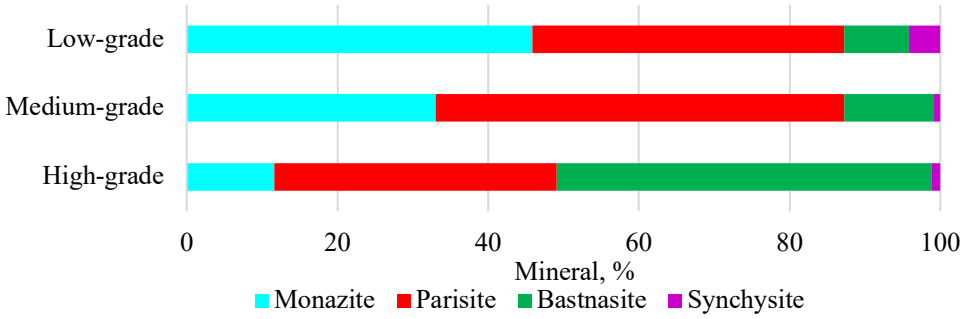

Fig. 3. Relative REMs content of different sample grades

Gangue and accessory minerals identified by automated-mineralogy in low-, medium- and high-grade samples are shown in Fig. 4, 5, and 6, respectively. The main gangue minerals are carbonates, including ferroan dolomite, ankerite, and calcite across all sample grades. Apatite, pyrite, and magnetite occur as accessory minerals with variable contents (Table 3). Calcite content of the high-grade sample is approximately 1.5 wt.%, compared with 25 wt.% in both the low- and medium-grade sample. The low-grade sample contains 33 wt.% ferroan dolomite, in contrast to 14 wt.% in the medium-grade and 23 wt.% in the high-grade sample. A consistent increase in ankerite is observed with increasing TREM content: 32 wt.% in the low-grade sample, 45 wt.% in the medium-grade sample, and 56 wt.% in the high-grade sample. Apatite is most abundant in the medium-grade sample (5.6 wt.%), whereas it accounts for 2.3 wt.% and 1.1 wt.% in the low- and high-grade samples, respectively. The high-grade sample contains the highest barite content (4.9 wt.%), compared with 0.6 wt.% in the low-grade sample and 1.4 wt.% in the medium-grade sample. Chlorite-Fe-Mg content remains similar in the low- and medium-grade sample (0.5 wt.%) but increases to 1.7 wt.% in the high-grade sample. Magnetite shows a comparable trend, staying around 2 wt.% in the low- and medium-grade sample and increasing to 3.2 wt.% in the high-grade sample.

3.3.2. Elemental deportment

The elemental deportment analysis showed that, in the low-grade sample, Ce, Nd, and La are distributed between monazite and parisite, with monazite being the dominant host (Fig. 7). In the

medium -grade sample, REEs are mainly present in parisite with monazite as the secondary dominant phase. In the high-grade sample, Ce and La are mostly concentrated in bastnäsite, while Nd is distributed between bastnäsite, parisite and monazite. Synchysite hosts 6%, 4% and 5% of Nd in the low-, medium-, and high-grade sample respectively. Praseodymium (Pr) was excluded from the REMs distribution analysis as its concentration was below the EDS detection limit.

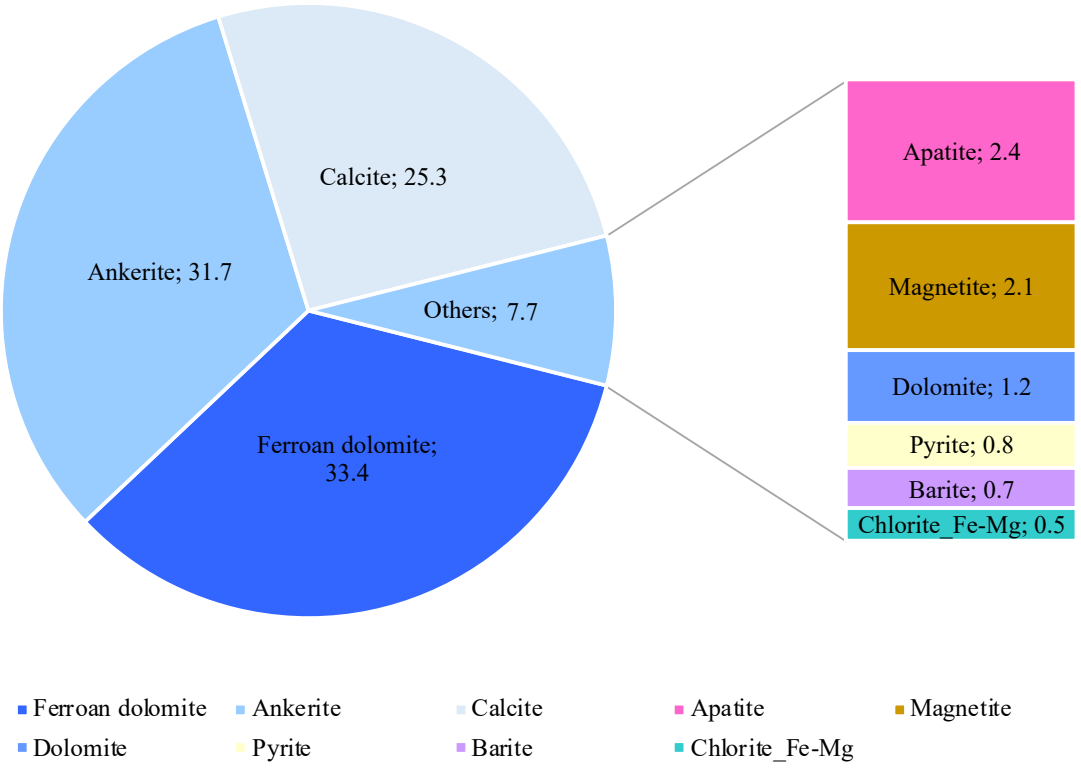

Fig. 4. Gangue and accessory minerals in the low-grade sample

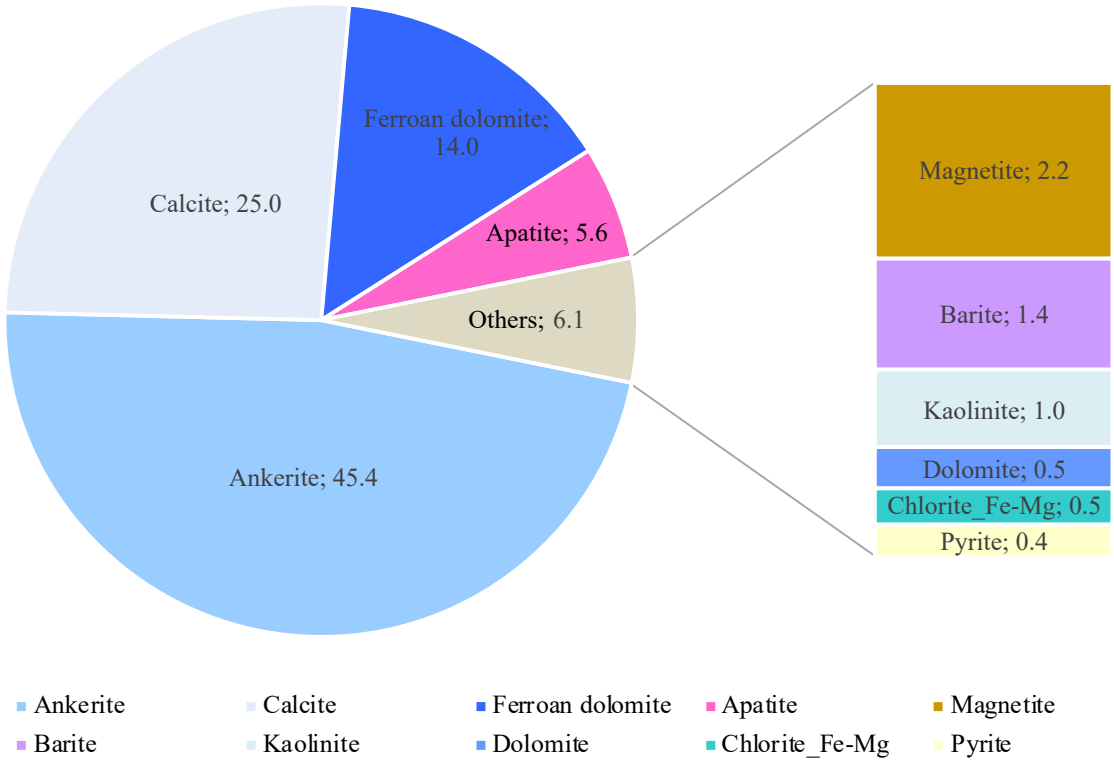

Fig. 5. Gangue and accessory minerals in the medium-grade sample

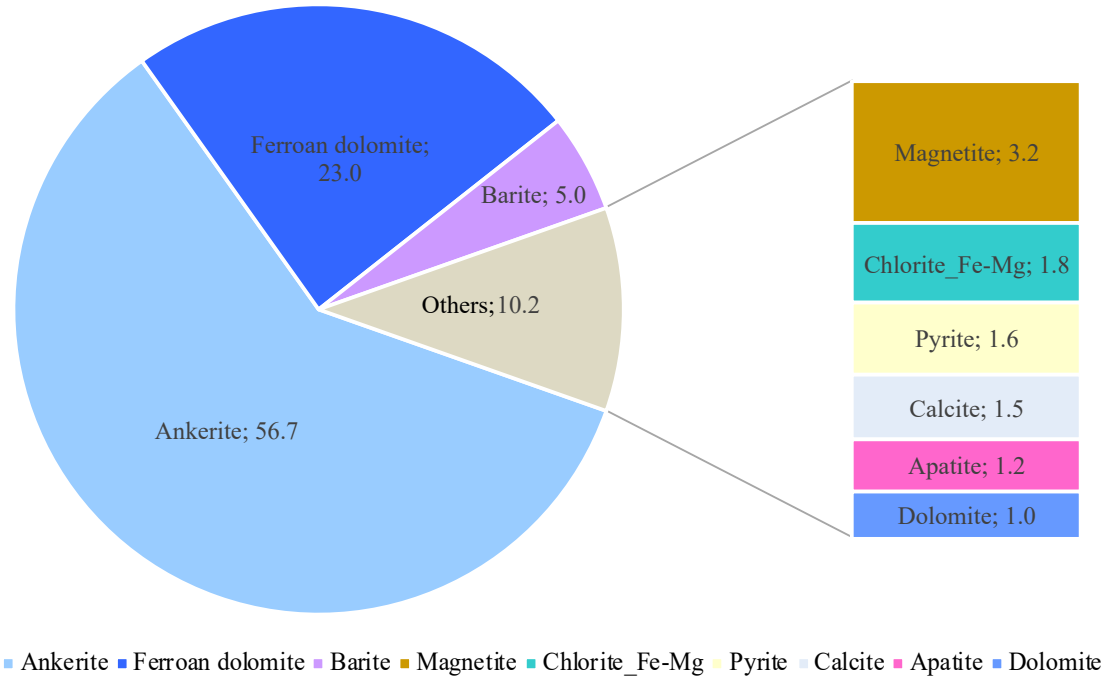

Fig. 6. Gangue and accessory minerals in the high-grade sample

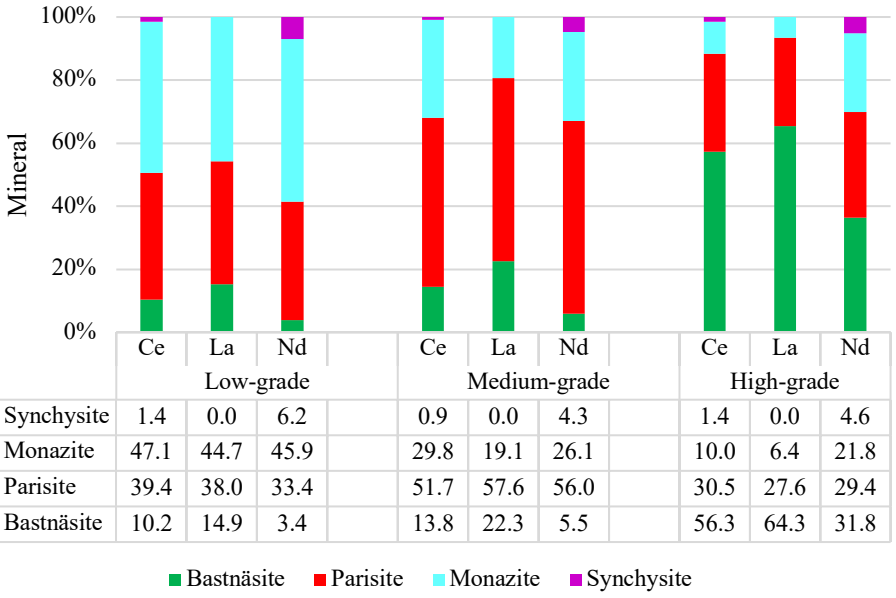

	Low-grade			Medium-grade			High-grade		
	Ce	La	Nd	Ce	La	Nd	Ce	La	Nd
Synchysite	1.4	0.0	6.2	0.9	0.0	4.3	1.4	0.0	4.6
Monazite	47.1	44.7	45.9	29.8	19.1	26.1	10.0	6.4	21.8
Parisite	39.4	38.0	33.4	51.7	57.6	56.0	30.5	27.6	29.4
Bastnäsite	10.2	14.9	3.4	13.8	22.3	5.5	56.3	64.3	31.8

Fig. 7. Elemental deportment of Ce, La and Nd by mineral in different sample grades

3.3.3. Liberation

The liberation classes for parisite grains in the low-, medium- and high-grade samples are presented in Fig. 8. Over 70% of the grains are classified as locked in the high-grade sample, decreasing to 63% in the medium-grade sample. In the low-grade sample, the proportions of locked and composite parisite grains are nearly equal at around 50%, while about 1% of the grains are liberated. The liberated grains in the medium- and high-grade samples account for 0.8%.

The liberation classes for bastnäsite grains in the low-, medium- and high-grade samples are presented in Fig. 9. In the low-grade sample, locked bastnäsite grains make up approximately 90%, while liberated grains account for only 1%. The medium- and high-grade samples each contain about 30% locked grains, with comparable proportions of composite grains as well. The high-grade sample has the highest amount of liberated bastnäsite grains (2.7%).

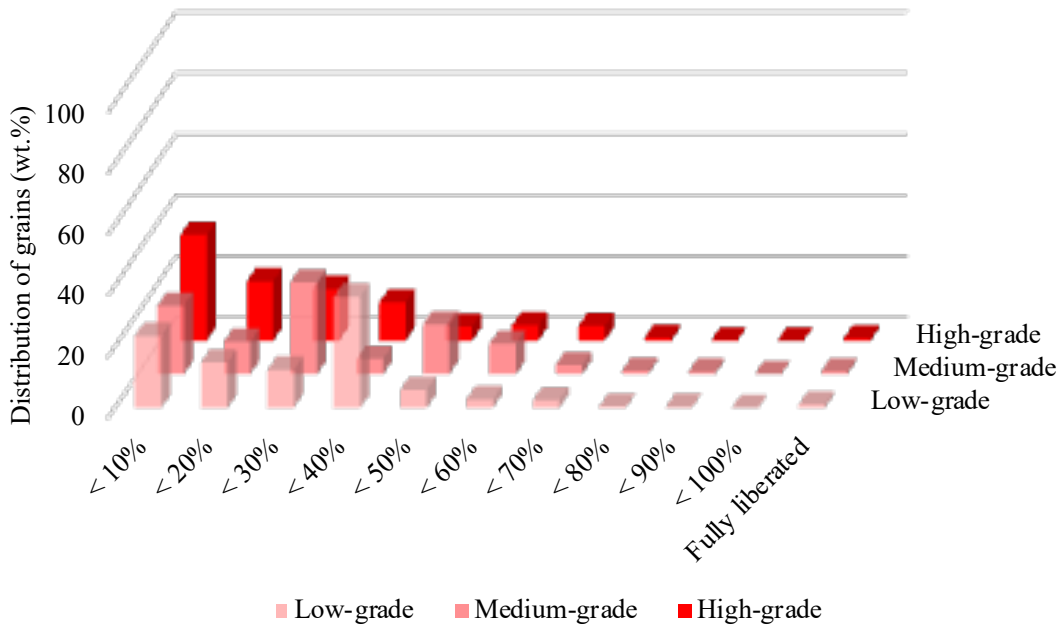

Fig. 8. Liberation classes of parisite by partial perimeter

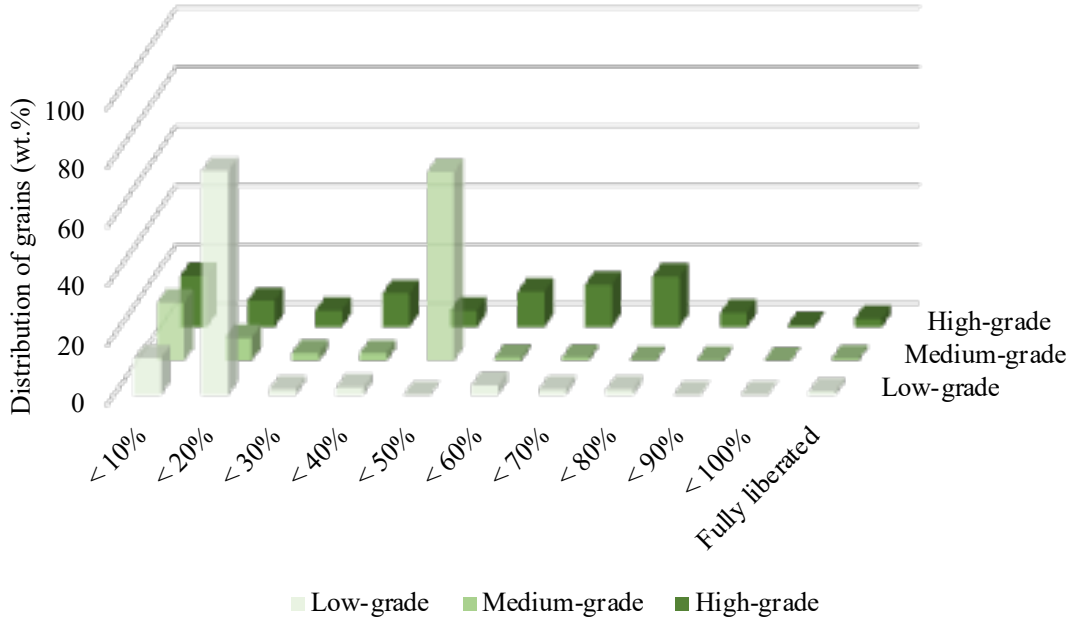

Fig. 9. Liberation classes of bastnäsite by partial perimeter

The liberation classes for monazite grains in the low-, medium- and high-grade samples are presented in Fig. 10. The medium-grade sample contains the highest proportion of locked monazite grains (44%), compared to 27% in the low-grade and 24% in the high-grade sample. Composite grains make up 53% of the medium-grade sample, while the low- and high-grade samples each contain approximately 60%. High-grade sample has the highest number of liberated monazite particles (14%), followed by low-grade (8%) and medium-grade sample (2%).

The liberation classes for synchysite grains in the low-, medium- and high-grade samples are presented in Fig. 11. In the low-grade sample, 48% of synchysite grains have less than 10% exposed partial perimeter, while locked grains account for 54% of all synchysite grains. For the medium- and high-grade samples, the proportion of grains with less than 10% exposed partial perimeter increases to 70% and 64%, respectively. The total proportion of locked grains in the medium- and high-grade samples is 91% in the medium-grade sample and 85% in the high-grade sample.

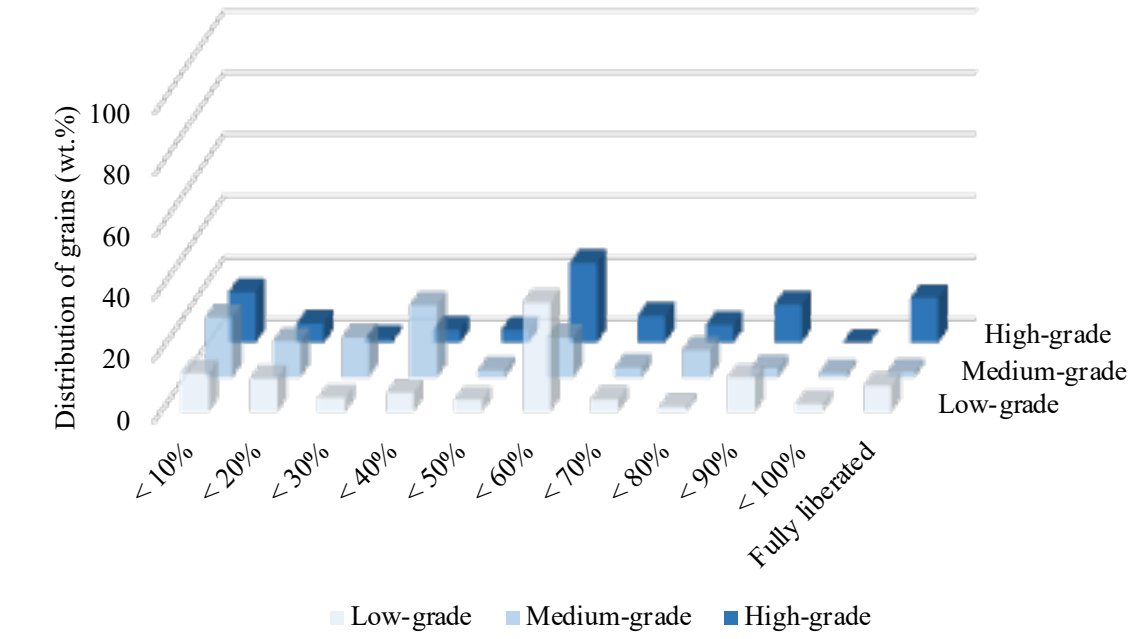

Fig. 10. Liberation classes of monazite by partial perimeter

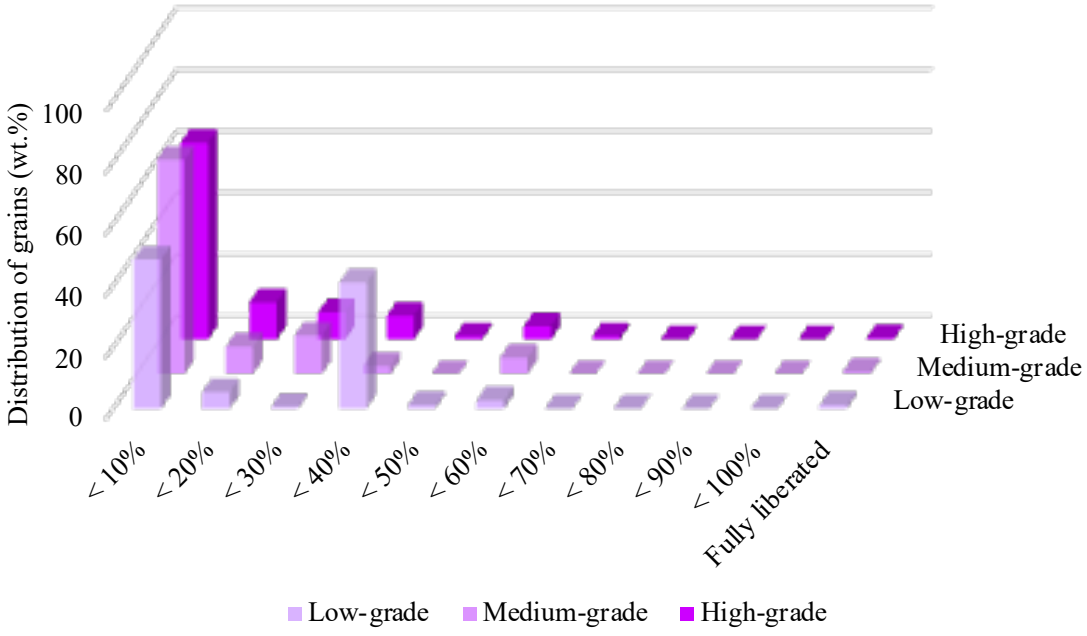

Fig. 11. Liberation classes of synchysite by partial perimeter

The liberation classes for magnetite grains in the low-, medium- and high-grade samples are presented in Fig. 12. Fully liberated magnetite grains are most abundant in the medium-grade sample (14%), followed by the high-grade sample (10%), while the low-grade sample contains only 5%. The proportion of locked magnetite grains follows the same trend, with 22% in the medium-grade sample, 20% in the high-grade sample, and 12% in the low-grade sample. Insights into the potential for magnetic separation should also be evaluated in relation to the mineral association data.

The grain size distribution of magnetite and REMs sub-groups in the low-grade sample is presented in Fig. 13. Synchysite was excluded from this part of the analysis because all detected grains were smaller than 5 µm, which likely represent single pixels rather than true mineral grains. Approximately 91% of parisite-Ce grains are finer than 15 µm, 7% of the grains fall within the 15–25 µm range while only 2% of them are distributed between 25 and 50 µm. The grain size distribution indicates that approximately 84% of parisite–Ce–La grains are finer than 15 µm, about 11% occur in the 15–25 µm size

fraction, and only ~3% are present in each of the 25–50 µm and 50–100 µm size ranges. Bastnäsite–Ce–La and monazite–Ce exhibit similar grain size distributions, with approximately 87% of their grains occurring in the <15 µm size fraction. Magnetite grains predominantly occur at relatively coarser sizes, with 77% of the grains finer than 15 µm. Approximately 14% fall within the 15–25 µm size fraction, while the remainder is distributed between the 25–50 µm and 50–100 µm size ranges.

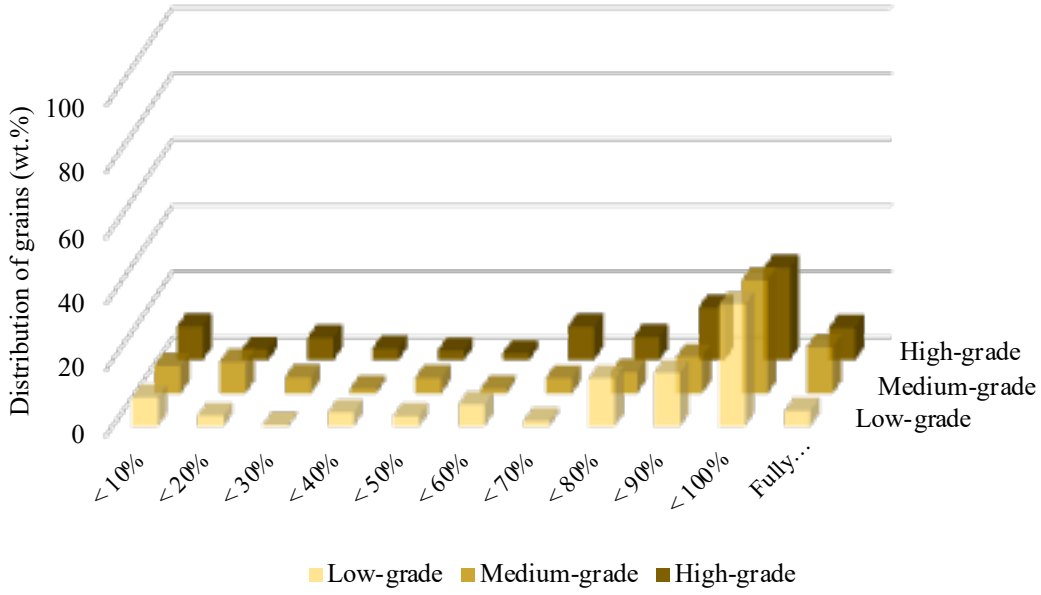

Fig. 12. Liberation classes of magnetite by partial perimeter

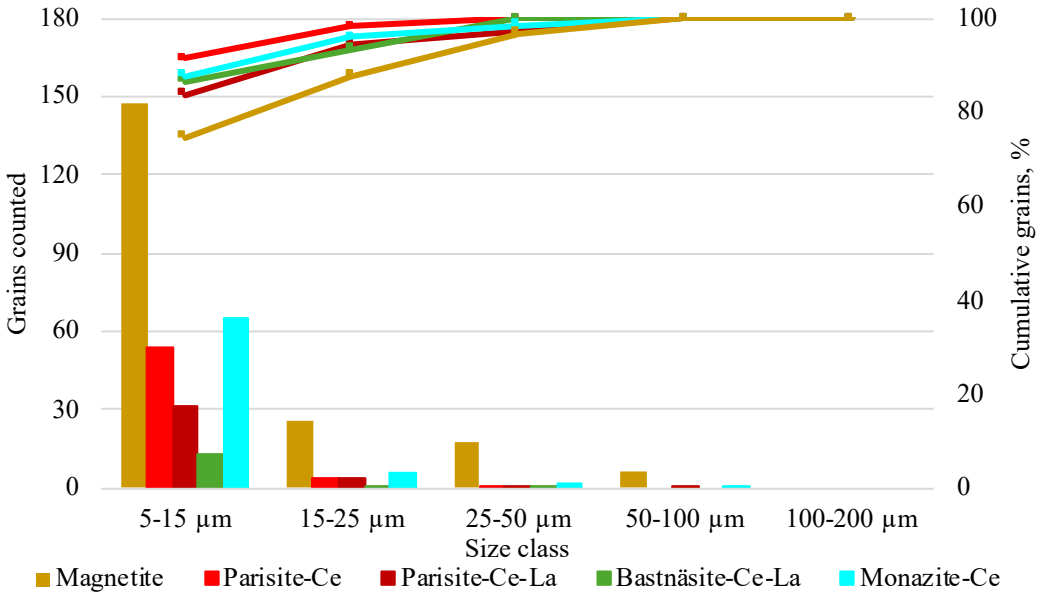

Fig. 13. Grain size distribution of REMs (sub-groups) in the low-grade sample. Bars show the number of counted grains in each size class, while lines represent the cumulative grain percentage

The grain size distribution of REMs sub-groups in the medium-grade sample is presented in Fig. 14. Approximately 90% of parisite-Ce grains are finer than 15 µm, and 94% of the grains are smaller than 25 µm. Approximately, 5% of the parisite-Ce grains fall within the range of 25–50 µm. The grain size distribution shows that 85% of parisite-Ce-La grains are below 15 µm, with 93% below 25 µm. Approximately, 6% of the parisite-Ce-La grains fall within the range of 25–50 µm. Bastnäsite-Ce-La grains occur predominantly at sizes below 15 µm (91%), with 94% smaller than 25 µm. Only ~3% are present in each of the 25–50 µm and 50–100 µm size ranges. Monazite-Ce grains are present at coarser size ranges 81% finer than 15 µm and 92% below 25 µm. Approximately, 6% of the monazite-Ce grains

fall within the range of 25–50 µm. The magnetite grain population is dominated by particles smaller than 15 µm (76%), with a further 15% distributed in the 15–25 µm fraction. Only minor proportions occur in the 25–50 µm (4%) and 50–100 µm (2%) size ranges.

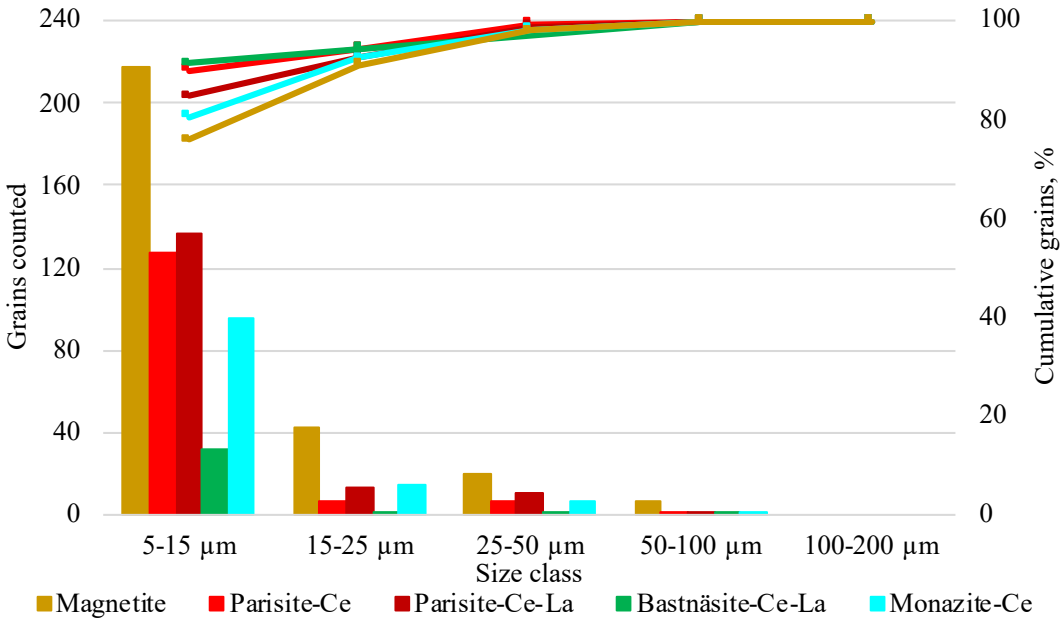

Fig. 14. Grain size distribution of REMs (sub-groups) in the medium-grade sample. Bars show the number of counted grains in each size class, while lines represent the cumulative grain percentage

The grain size distribution of REMs sub-groups in the high-grade sample is presented in Fig. 15. Approximately 92% of parisite-Ce grains are finer than 15 µm, and all grains are smaller than 50 µm. The grain size distribution of parisite-Ce-La indicates that 87% of grains are below 15 µm, with 99% smaller than 50 µm. Bastnäsite-Ce-La grains occur predominantly at sizes below 15 µm (81%), with 94% finer than 25 µm. Monazite-Ce grains exhibit a similar size distribution, with 84% finer than 15 µm and 95% below 25 µm. Magnetite grains are predominantly finer than 15 µm, accounting for 77% of the population, while an additional 14% occur in the 15–25 µm size range. Grains in the 25–50 µm fraction represent only minor contributions, at 8%.

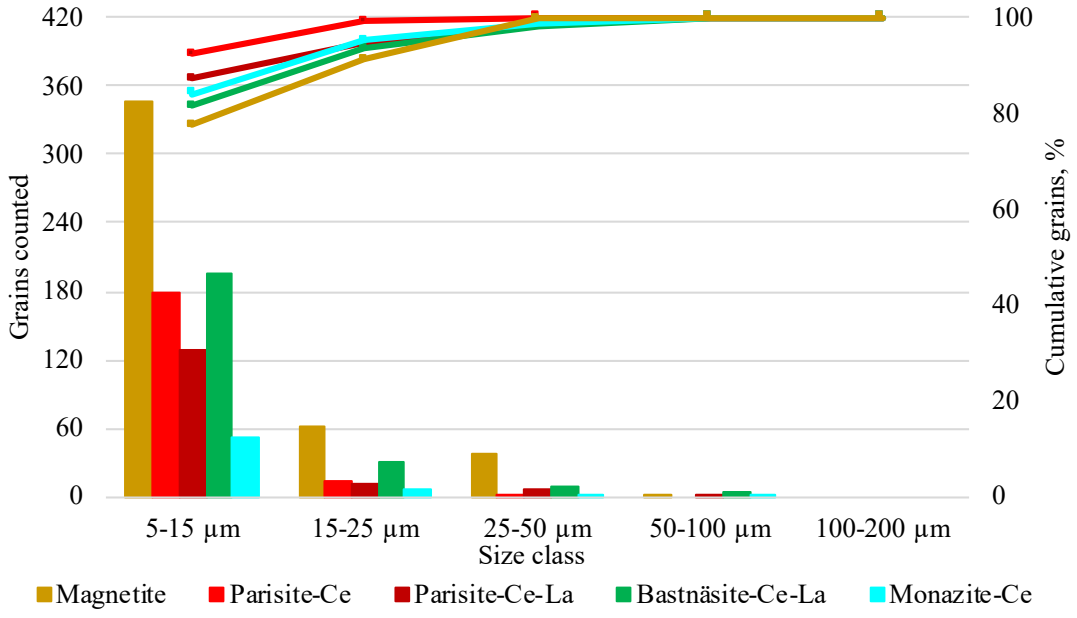

Fig. 15. Grain size distribution of REMs (sub-groups) in the high-grade sample. Bars show the number of counted grains in each size class, while lines represent the cumulative grain percentage

3.3.4. Mineral associations

Mineral associations are presented for magnetite and each main REMs sub-type, showing the relationships with gangue minerals and with the other main REMs sub-types (parisite-Ce, parisite-Ce-La, bastnäsite-Ce-La, monazite-Ce and synchysite-Ce are combined as TREM). The analysis focuses on target minerals because their mineralogical characteristics and associations directly control the efficiency and selectivity of beneficiation processes. This targeted approach enables a more accurate assessment of liberation and potential separation challenges relevant to process design. Mineral associations for parisite-Ce grains in low-, medium- and high-grade sample material are presented in Fig. 16. The highest free surface for parisite-Ce grains was observed in the low-grade sample (20%) followed by high- (13%) and medium-grade (12%) sample. Parisite-Ce is mainly associated to the other REMs sub-types and shows a comparable association (~ 45-50%) across all sample grades. Its association with ferroan dolomite was greatest in the high-grade sample, 10.7%, decreasing to 4.5% in the low-grade and 1.6% in the medium-grade samples. A parallel trend was observed for ankerite, with a 16% association in the high-grade sample and 3% and 4.3% in the low- and medium-grade sample, respectively. The association between parisite-Ce and calcite was highest in the low-grade sample (7.8%), followed by the medium-grade sample (5.3%), and lowest in the high-grade sample (0.8%). It exhibited a 2.1% association with barite in the medium-grade sample, with no detectable association in the low- or high-grade sample. The association between parisite-Ce and magnetite was similar in the low- and high-grade samples, both around 1%, while it increased to 2.6% in the medium-grade sample. The highest association of chlorite-Fe-Mg was detected in medium-grade sample (1.2%) followed by high- (0.8%) and low-grade sample (0.5%). Mineral phases present in minor concentrations (<0.1 wt%) are grouped under 'others' in the product classifications. Additionally, the samples contained unclassified fractions due to agglomerates formed during sample preparation. These agglomerates primarily consist of a matrix phase composed of Ca, Fe, Mg, O, and Si.

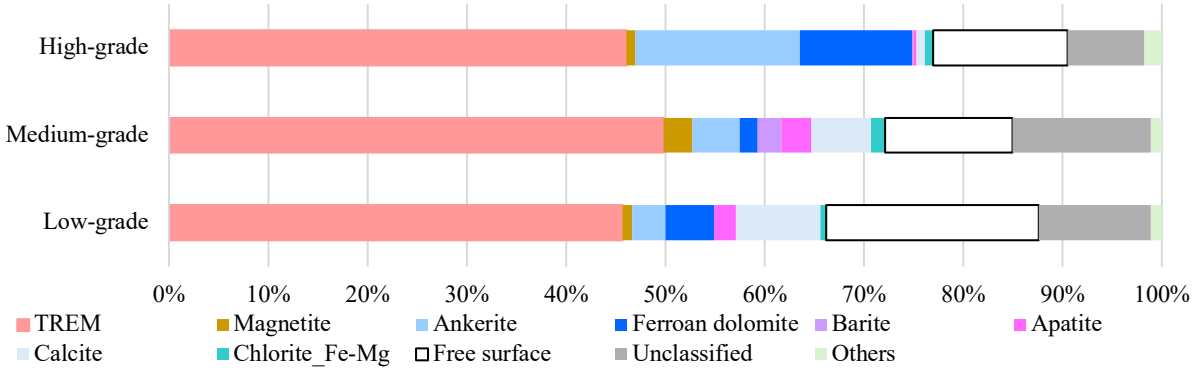

Fig. 16. Mineral associations for parisite-Ce grains in low-, medium- and high-grade samples

Mineral associations for parisite-Ce-La grains in low-, medium- and high-grade sample are presented in Fig. 17. The highest free surface for parisite-Ce-La grains was observed in the medium-grade sample (16%) followed by high-grade (14%) and low-grade (13%) sample. Parisite-Ce-La is mainly associated to the other REMs sub-types across all sample grades and the low-grade sample exhibited the strongest association with them while it is slightly lower for the medium- and high-grade sample. The associations of parisite-Ce-La with ankerite and ferroan dolomite were highest in the high-grade sample, at 7.8% and 5.9%, respectively, while their associations in the low- and medium-grade sample were negligible. Parisite-Ce-La showed the lowest association with calcite in the high-grade sample (1%), while the low- and medium-grade sample exhibited higher associations of 4.6% and 3.7%, respectively. The association with magnetite was highest in the medium-grade sample (1.6%), followed by the high-grade (0.7%) and low-grade sample (0.1%). Chlorite-Fe-Mg showed the highest association in low-grade sample (1%) followed by medium- (0.8%) and high-grade sample (0.4%).

Mineral associations for bastnäsite-Ce-La grains in low-, medium- and high-grade sample are presented in Fig. 18. The highest free surface for bastnäsite-Ce-La grains was observed in the high-grade sample (32%) followed by low-grade (14%) and medium-grade (10%) sample.

Bastnäsite-Ce-La is mainly associated to the other REMs sub-types across all sample grades and the low-grade sample exhibited the highest degree of association with them, while the high-grade sample displayed the lowest. The highest free surface for this REMs sub-type grains was observed in the high-grade sample followed by low-grade and medium-grade sample. Like parisite-Ce-La, the association of bastnäsite-Ce-La with ankerite and ferroan dolomite was highest in the high-grade sample (3.5% and 2.6%, respectively), while such associations were negligible in the low- and medium-grade samples. The magnetite association was highest in the medium-grade sample (0.9%), followed by the high-grade (0.7%) and low-grade sample (0.2%). Chlorite-Fe-Mg showed the highest association in medium-grade sample (2%) followed by low- (1.3%) and high-grade sample (0.5%).

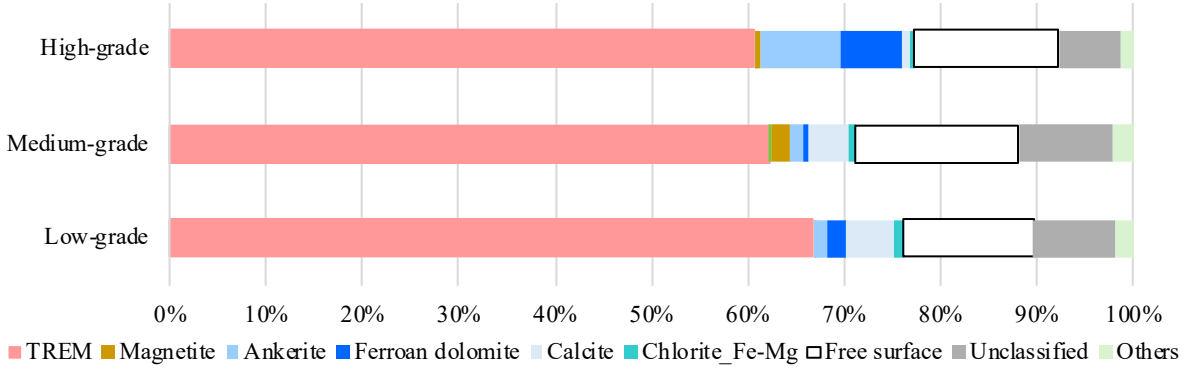

Fig. 17. Mineral associations for parisite-Ce-La grains in low-, medium- and high-grade samples

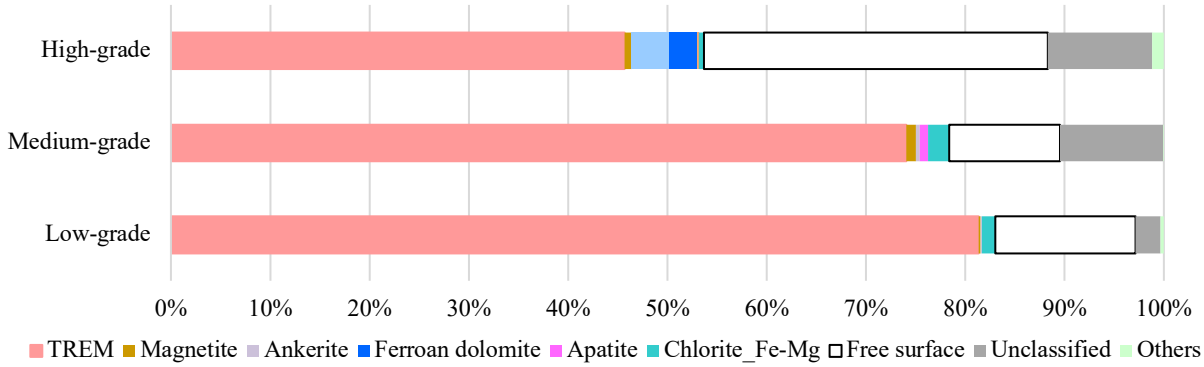

Fig. 18. Mineral associations for bastnäsite-Ce-La grains in low-, medium- and high-grade samples

Mineral associations for monazite-Ce grains in low-, medium- and high-grade sample are presented in Fig. 19. The highest free surface for monazite-Ce grains was observed in the low- and high-grade sample (~ 40%), followed by medium-grade (18%). Monazite-Ce grains in the medium- and low-grade sample were mainly associated to apatite at 18 and 9%, respectively. Its associations to calcite were 8% in the low-grade and 11% in the medium-grade sample, while negligible in the high-grade sample. Monazite-Ce grains in the high-grade sample were primarily associated with other REMs (10.4%), followed by ankerite (7%), ferroan dolomite (6%), and both chlorite-Fe-Mg and apatite, each at approximately 4%. It showed the highest association with magnetite grains in the low-grade sample (4%), followed by 2.8% in the medium-grade and 1.5% in the high-grade sample.

Mineral associations for synchysite-Ce grains in low-, medium- and high-grade sample are presented in Fig. 20. The highest free surface for synchysite-Ce grains was observed in the low-grade (36%), followed by medium- and high-grade (each ~ 26%). Synchysite-Ce is mainly associated to the other REMs sub-types across all sample grades. It exhibited the strongest association to the other REMs in both the low- and high-grade samples (over 60%), whereas the medium-grade sample showed a reduced level of association (50%). Its association to magnetite was detected only in the high-grade sample (0.7%), whereas calcite associations appeared only in the medium-grade sample (4%).

Synchysite-Ce associated to chlorite-Fe-Mg was 1.2% in the high-grade sample and negligible in the low- and medium-grade sample.

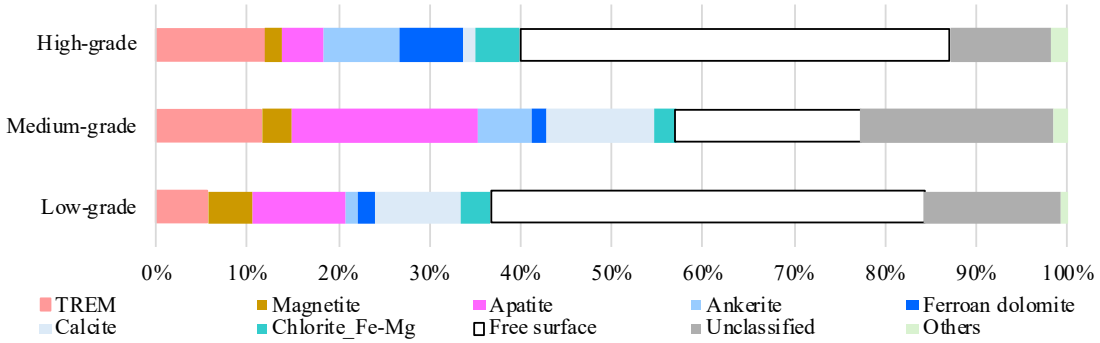

Fig. 19. Mineral associations for monazite-Ce grains in low-, medium- and high-grade samples

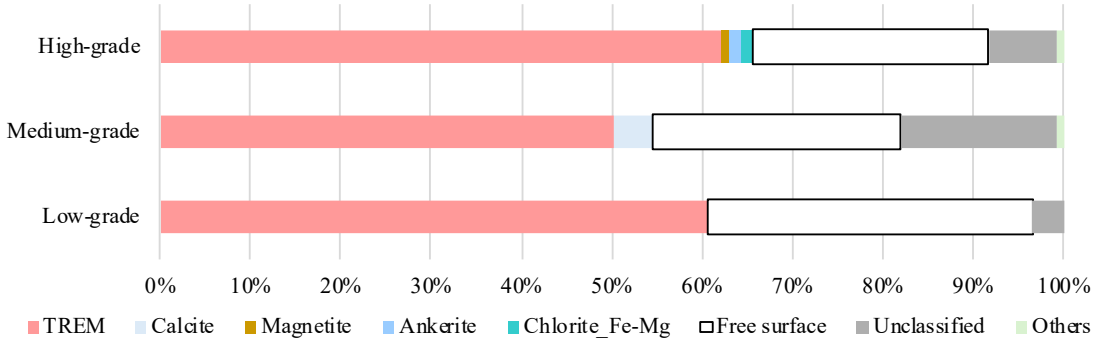

Fig. 20. Mineral associations for synchysite-Ce grains in low-, medium- and high-grade samples

Mineral associations for magnetite grains in low-, medium- and high-grade sample are presented in Fig. 21. The low- and high-grade sample have similar free surfaces (53%), whereas the medium-grade sample shows a slightly lower value (49%). Magnetite grains in the low- and medium-grade sample are mainly associated to calcite (10%), while they are mainly associated to ankerite in the high-grade sample (12%). Magnetite grains in both the low- and high-grade samples show a 2% association with REM, whereas the grains in the medium-grade sample exhibit the highest REMs association (6%) among the sample grades. Chlorite-Fe-Mg was the highest in the high-grade sample (2%) while it is negligible in the low- and medium-grade sample.

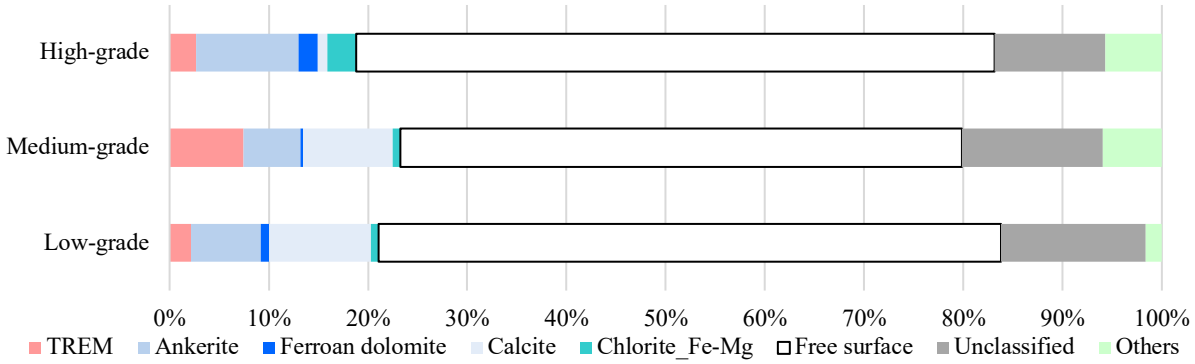

Fig. 21. Mineral associations for magnetite grains in low-, medium- and high-grade samples

4. Discussion

4.1. Processing behaviour interpreted through modal mineralogy

Accurate identification and quantification of both target and gangue minerals in the feed material are essential for determining the sample's processing route (Petruk, 2000; Lotter, 2011). Most rare earth

deposits are complex and require a combination of physical and physico-chemical processing methods, with flotation being the technique for their recovery from fine grained ores (Ferron et al., 1991; Marion et al., 2020). The following section presents a discussion of the sample grades with reference to their modal mineralogy as well as the surface and bulk characteristics of the target and gangue minerals.

The dominant REMs vary across sample grades. As shown in section **3.3.1**, monazite is the main REMs in the low-grade sample, whereas parisite dominates the medium-grade sample. In the high-grade sample, both bastnäsite and parisite are the main REMs. Monazite (a phosphate mineral) and the other main target minerals (carbonate minerals) belong to different mineral families and may therefore require distinct separation methods or varying conditions within the same method, such as the application of specific reagents during flotation (Marion et al., 2020). These target minerals possess relatively high densities (greater than 3.9 g/cm^3), while the primary gangue minerals typically exhibit densities around 3 g/cm^3 or lower, suggesting that gravity separation could serve as an effective pre-concentration technique for these REMs (Table 4). Gravity separation techniques such as shaking tables, spiral concentrators, and conical separators are commonly used in combination with froth flotation at many rare earth mineral processing operations across China, which accounts for approximately 85% of global REEs processing (Jordens et al., 2013; European Commission, 2023). Calcite is one of the main gangue minerals in the low- and medium-grade sample with a density of 2.7 g/cm^3 making these sample grades more suitable for gravity separation compared to high-grade sample (Wills and Finch, 2016). Moreover, as the low- and medium-grade samples are relatively richer in monazite, the target mineral with the highest density, which enhances the density contrast and thereby increases the concentration criterion for effective separation (Wills and Finch, 2016).

Another shared characteristic of the REMs in the investigated sample is their paramagnetic nature, which requires high-intensity magnetic separation to recover them in the magnetic fraction (Wills and Finch, 2016). In REMs beneficiation, magnetic separation is commonly employed not only to concentrate paramagnetic REMs but also to remove magnetic gangue minerals such as iron oxides (Jordens et al., 2013). The magnetite content is approximately 2.2 wt.% in the low- and medium-grade sample, and 3.2 wt.% in the high-grade sample. Low-intensity magnetic separation (LIMS) can be employed to remove magnetite before proceeding to more selective separation steps (Jordens et al., 2014). This may help reduce unnecessary collector consumption caused by the formation of complexes between hydroxamates and iron ions released to the slurry by magnetite. However, based on the mineral association data, approximately 2 wt.% of the TREM in both the low- and high-grade samples, and about 6 wt.% in the medium-grade sample, would be removed together with magnetite. TREM losses during magnetic separation may be higher due to the inherently imperfect nature of the separation processes (Wills and Finch, 2016). Modal mineralogy alone is insufficient to further interpret these results and a more detailed discussion is provided in the following sections. Potential processing routes for the different sample grades should be determined not only based on modal mineralogy but also on liberation and mineral association data, as separation methods that exploit differences in the physical characteristics of minerals tend to become less efficient with decreasing particle size (Drzymala, 2007).

The main gangue mineral in the medium- and high-grade samples is ankerite, followed by calcite in the medium-grade and ferroan dolomite in the high-grade sample. Ferroan dolomite, where a minor portion of Mg^{2+} in dolomite is substituted by Fe^{2+} ions (Deer et al., 2013), is the dominant gangue mineral in the low-grade sample, followed by ankerite and calcite. The types of atoms exposed on the surfaces of ankerite, calcite, and ferroan dolomite differ depending on each mineral's composition (Deer et al., 2013). Calcite surface exposes calcium and oxygen atoms, while ferroan dolomite exposes calcium, magnesium, and iron atoms. Ankerite, in addition to calcium, exposes iron, magnesium, and manganese atoms (Azizi and Larachi, 2018). Along with the anions and cations present on the mineral surface, ionic species released into solution during wet processing, are also determined by the mineral's composition. Consequently, surface charging is governed by the dissolution or adsorption of ions at the mineral–solution interface (Zhang et al., 2013). Understanding the surface characteristics will facilitate the selection of suitable reagents for the efficient separation of target REMs from these gangue minerals via flotation (Marion at al., 2020).

There are two types of adsorptions in flotation: physisorption, which occurs through electrostatic attraction, and chemisorption, which occurs via covalent or coordinate bonds between the surface

species and the reagents (Leja, 1982). Since gangue minerals typically have the same surface charge (positive) as REMs, the use of collectors that rely primarily on physisorption is likely to be challenging (Marion et al., 2020). Hydroxamates and carboxylates are the most used collectors in REMs flotation (Gajendra et al., 2025). Hydroxamates are considerably more selective than fatty acids due to differences in the stability of the complexes formed by these two collector groups with metal cations present at the mineral surface (Liu et al., 2023). The most stable complexes are formed with Fe^{3+}, Al^{3+}, Cu^{2+}, and Pb^{2+}, while Ca^{2+}, Mg^{2+}, and Ba^{2+} form the weakest complexes (Marion et al., 2020). Rare earth metal cations fall in between these two groups in terms of complex stability. Additionally, the stability constant of Fe^{2+} is higher than that of Ca^{2+} and the selectivity increases with the magnitude of the difference in stability constants of the complexes formed with surface cations (Table 5) (Marion et al., 2020). Azizi and Larachi (2018) investigated the surface interactions and adsorption mechanisms of an alkyl hydroxamic acid collector (Aero 6493) and a sodium silicate (SS) depressant on calcite, dolomite, and ankerite, providing valuable insights into the flotation behavior of various valuable minerals associated to carbonatite gangues. The researchers demonstrated through microflotation tests that ankerite exhibited higher recoveries than dolomite and calcite across all tested pH values (Fig. 22). They also performed zeta potential measurements and density functional theory (DFT) simulations, which revealed that the stronger affinity of ankerite for the collector (Aero 6493) can be attributed to the presence of Fe and Mn in its crystal structure. As mentioned above, Fe and Mn are transition metals that tend to form more stable complexes with hydroxamic acid collectors unlike Ca and Mg (Jordens et al., 2014; Nduwa-Mushidi and Anderson, 2017; Azizi and Larachi, 2018). The high-grade sample, which contains the highest proportion of ankerite and the second highest ferroan dolomite among the examined sample grades (80 wt.% in total), may promote hydroxamate adsorption onto gangue minerals, leading to undesirable gangue recovery. However, such collector adsorption can be mitigated using an appropriate depressant, such as SS (Azizi and Larachi, 2018). SS is one of the most used depressants in REMs flotation, including at Bayan Obo, China (Kim et al., 2025). Its negatively charged colloidal particles adsorb onto the calcium- and barium-hydroxylated complexes on the surfaces of gangue minerals such as fluorite, barite, and calcite, forming hydrophilic films and thereby depressing them. In addition, it can adsorb excess calcium and magnesium ions from the solution, preventing their consumption of the collector (Liu et al., 2023). It is worth noting at this stage that the high-grade sample contains the highest barite content (5 wt.%) besides ankerite and ferroan dolomite.

Espiritu et al. (2018) investigated the effects of dissolved dolomite species on bastnäsite, monazite, and dolomite, examining the floatability and molecular-scale interactions in the presence of benzohydroxamate

Table 5. Stability constants of metal acetohydroxamate complexes at 20 °C (Nduwa-Mushid and Anderson, 2017)

Cation	$LogK_1$	$LogK_2$	$LogK_3$
Ca^{2+}	2.4		
Mn^{2+}	4.0	2.9	
Cd^{2+}	4.5	3.3	
Fe^{2+}	4.8	3.7	
Co^{2+}	5.1	3.8	
Ni^{2+}	5.3	4.0	
Zn^{2+}	5.4	4.2	
Pb^{2+}	6.7	4.0	
Cu^{2+}	7.9		
La^{3+}	5.16	4.17	2.55
Ce^{3+}	5.45	4.34	3.0
Sm^{3+}	5.96	4.77	3.68
Gd^{3+}	6.10	4.76	3.07
Dy^{3+}	6.52	5.39	4.04
Yb^{3+}	6.61	5.59	4.29
Al^{3+}	7.95	7.34	6.18
Fe^{3+}	11.42	9.68	7.23

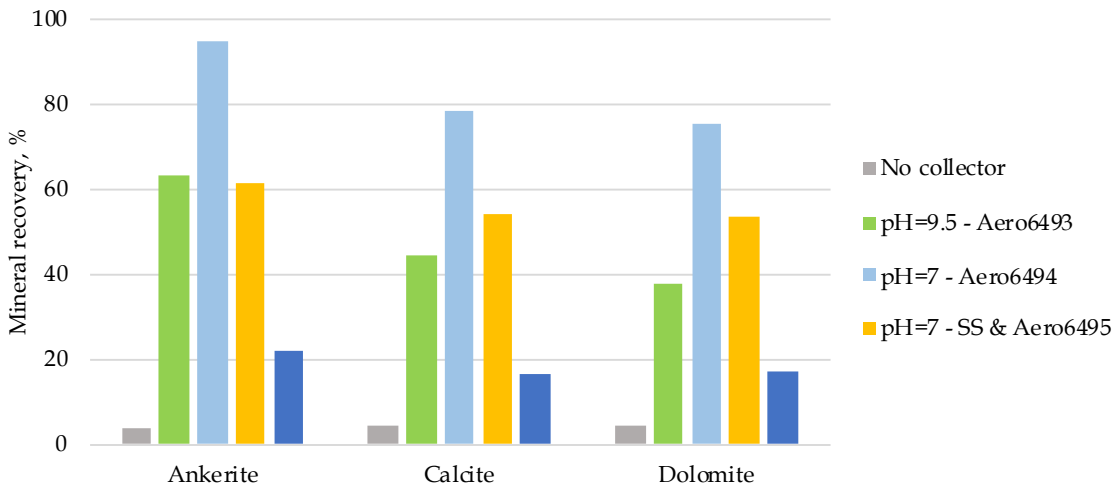

Fig. 22. Micro-flotation tests were conducted on calcite, dolomite, and ankerite using Aero 6493 and SS at pH values of 7 and 9.5 (adapted from Azizi and Larachi, 2018)

(BHA). The researchers observed a decrease in the floatability of both bastnäsite and monazite in the presence of dolomite, with the effect being more pronounced for bastnäsite (Fig. 23). To detect the precipitated species on the mineral surfaces, the samples were analyzed using X-ray photoelectron spectroscopy (XPS). The analysis revealed the presence of $Ca(OH)_2$, $MgCO_3$ and $CaCO_3$ and Ca^{2+}on the monazite surfaces. These adsorbed ions or precipitated species on the surfaces of REMs can serve as new sites for collector adsorption. However, the interaction between these species and the collector is less favorable than that between the mineral surface and the collector, leading to a decrease in mineral recovery. Another possible reason for the decrease in recovery is the presence of solvated dolomite (ionic) species in the solution, which can consume the collector through complexation (Espiritu et al., 2018). Thus, low-grade sample, with the highest ferroan dolomite content, requires prevention of precipitate adsorption on target mineral surfaces before conditioning with the collector (BHA).

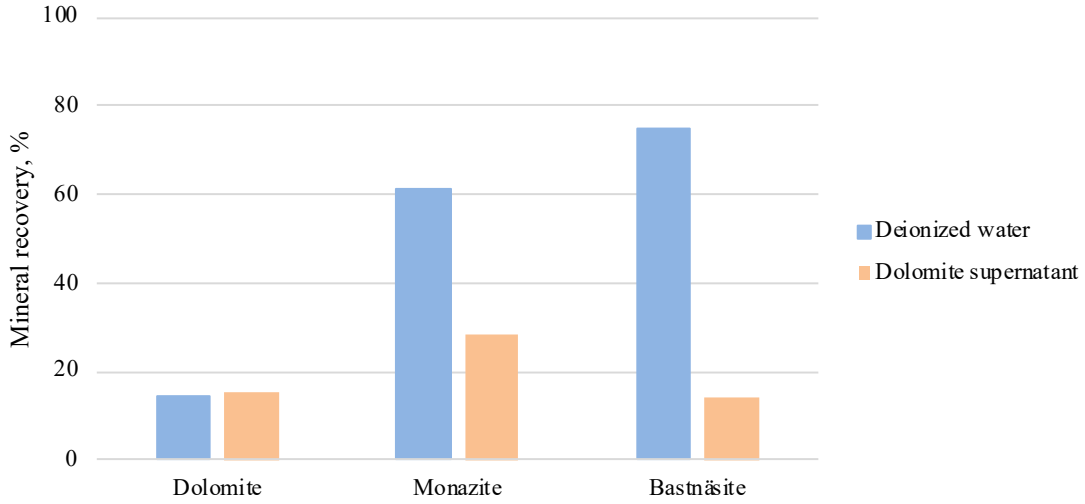

Fig. 23. Microflotation results of dolomite, monazite, and bastnäsite obtained using benzohydroxamic acid (BHA) in deionized water and dolomite supernatant at pH 9 (adapted from Espiritu et al., 2018)

Phosphate minerals in the samples studied in this paper occur primarily as monazite and apatite; however, apatite is not considered a REEs target mineral in this deposit due to its negligible REEs content. (Dahlgren, 2019). Medium-grade sample material has the highest apatite content among the other sample grades. Nduwa-Mushidi and Anderson (2017), provided a basis on separation of monazite from its associated minerals such as apatite, ilmenite, rutile, zircon and quartz using flotation. In addition to microflotation tests, the researchers measured zeta potential and adsorption densities of

octanohydroxamic (OHA) acid on the surface of each mineral and discussed their flotation behavior. Zeta potential measurements indicated that adsorption occurred through chemisorption on both monazite and apatite. Adsorption isotherm experiments further revealed that increasing the temperature from 25 °C to 80 °C enhanced the adsorption density on monazite surfaces by approximately 3.5-fold, with a similar trend observed for apatite. Microflotation results showed that monazite and its gangue minerals exhibited comparable flotation responses when OHA was used as the collector. In addition, monazite exhibited maximum floatability at pH values between 7.5 and 10. In contrast, apatite floatability increased progressively with rising pH, reaching its maximum at pH 12.6. Considering the literature, two main conclusions can be drawn. First, monazite flotation requires higher temperatures than the other target minerals, likely due to its lower solubility, making the flotation of low-grade samples more costly. Second, fine-tuning of flotation parameters (such as pH) is necessary to achieve efficient monazite separation in the low- and medium-grade samples, which have apatite/TREM ratios of 2.5 and 2, respectively (Nduwa-Mushidi and Anderson, 2017).

A summary of separation potential for different methods, along with grade-specific considerations based on mineralogical characteristics is given in Table 6. Gravity separation techniques are generally cost-effective, with low capital and operational expenses since they do not require reagents. They are also environmentally friendly and relatively easy to implement. Although specific gravity is a key factor in gravity separation, particle size and shape also significantly influence the process (Wills and Finch, 2016). In REM processing, magnetic separation is applied in various ways depending on the ore type. They, used alongside gravity separation, play a key role in monazite beneficiation from beach sands. They help remove strongly magnetic minerals like magnetite before finer separation stages and are also applied to separate paramagnetic monazite especially from non-magnetic heavy minerals such as zircon and rutile (Jordens et al., 2013). Potential processing routes for the different sample grades should be determined not only based on modal mineralogy but also on liberation and mineral association data, as separation methods that exploit differences in the physical characteristics of minerals tend to become less efficient with decreasing particle size (Drzymala, 2007).

Table 6. Separation potential of different methods, along with grade-specific considerations based on mineralogical characteristics

Sample grade	Low	Medium	High
Mineralogical composition	- Monazite-rich - Carbonate-dominated gangue (ferroan dolomite, ankerite, calcite)	- Monazite- and parisite-rich - Carbonate-dominated gangue (ferroan dolomite, ankerite, calcite) - Apatite-rich	- Bastnäsite- and -parisite rich - Carbonate gangue (ferroan dolomite, ankerite) - Barite-rich
Gravity separation	Potential: Pre-concentration stage **Key Factor:** Higher calcite content enhances density contrast	Potential: Pre-concentration stage **Key Factor:** Higher calcite content enhances density contrast	Potential: Limited **Key Factor:** Lower calcite content may reduce efficiency
Magnetic separation	Potential: Pre-concentration stage **Key Factor:** More liberated magnetite with weak association to REM	Potential: Limited **Key Factor:** Stronger magnetite–REMs associations may increase losses	Potential: Pre-concentration stage **Key Factor:** Higher magnetite content and better liberation
Flotation	Potential: Concentration **Key Factor:** Phosphate nature of monazite may require tailored conditions	Potential: Concentration stage **Key Factor:** Higher apatite content and apatite-monazite associations may reduce selectivity	Potential: Concentration **Key Factor:** Elevated Fe, Mn, and Ba may require depressants or surface modifiers

4.2. Grade-specific elemental deportment and processing considerations

The elemental deportment analysis revealed clear variations in the distribution of REEs across different sample grades. Among the REEs present, Nd has the highest supply risk and economic significance due to its widespread use in permanent magnets followed by Pr, Ce and La (European Commission, 2023). In the low-grade sample, 46% of Nd is hosted by monazite, with parisite as a secondary carrier, indicating that the separation process should target both phosphate and carbonate REMs. As the grade increases to the medium level, target elements are mainly concentrated in parisite, indicating a shift in the dominant REMs from phosphate to carbonate phases. In the high-grade sample, Ce and La are predominantly hosted by bastnäsite, while Nd exhibits a more complex distribution among bastnäsite, parisite, and monazite. This progressive change in host mineralogy across sample grades suggests that REMs associations evolve with increasing grade, potentially leading to different responses under the same processing conditions. Synchysite, although a minor phase contributing 4–6% of the total Nd across all grades, remains a consistent secondary carrier. It may influence flotation selectivity to a limited extent due to its surface chemistry being similar to that of other carbonate REMs (Owens et al., 2018).

4.3. Insights into processing behavior from target and accessory mineral liberation

Size reduction is the most energy-intensive and, consequently, the costliest stage in mineral processing (Wills and Finch, 2016). The goal is to liberate target minerals from the gangue without excessive grinding, as over-grinding not only increases operational costs but also generates fine particles that can adversely affect processing efficiency during flotation (McIvor and Finch, 1991; Wills and Finch, 2016). Sufficient particle liberation is essential for the effective recovery of valuable minerals through separation processes, particularly froth flotation, where inadequate liberation can significantly reduce selectivity and overall recovery (Bradshaw, 2014).

At the current grind size (Fig. 1), parisite and synchysite grains in the low-grade sample, which account for approximately 45% of the total target mineral content, exhibited a higher degree of liberation compared to those in the medium- and high-grade sample. The liberation characteristics of monazite indicate that, although only about 8.5% of the grains are fully liberated, the additional 61% occurring as composite grains with more than 30% exposed perimeter suggests that a substantial portion of the monazite is still accessible for effective separation. These characteristics suggest that, although complete liberation has not been achieved, the current grind size is sufficient to promote potential recoverability of REMs in the low-grade sample.

As presented in Section 3.3.3, the medium-grade sample contains an REE assemblage dominated by parisite and monazite, which together account for 87% of the TREM content. Although fully liberated parisite grains represent less than 1% and 63% remain locked, its overall exposure and mineral associations indicate that efficient separation is still achievable, provided that appropriate beneficiation strategies are applied. Although around 70% of the synchysite grains possess less than 10% exposed perimeter, their frequent association with other REMs suggests that they may still be efficiently recovered. Among sample grades, medium-grade sample is the one with the lowest number of liberated monazite grains, which was consistent with the association data. The liberation characteristics together with mineral association data show that partially liberated monazite necessitates optimized comminution to increase recovery to acceptable values for this sample grade.

Unlike the lower-grade samples, bastnäsite serves as the main REM in the high-grade sample with 50% relative abundance. The high proportion of composite grains (65%) is likely to support acceptable recovery during flotation. Although a relatively high proportion of parisite grains remain locked, potentially limiting their separation efficiency, both parisite-Ce and parisite-Ce-La are primarily associated to other REMs and may still achieve acceptable recoveries at the current grind size. In the high-grade sample, monazite – a tertiary target mineral with roughly 10% relative abundance among the REMs – shows favorable liberation characteristics and is primarily associated to other REMs. Its separation potential should be significantly better than in the medium-grade sample. Therefore, the recovery of TREO in the flotation concentrates at the end of one rougher and two cleaner stages was similar for all sample grades, at approximately 70% (Appendix A3). Although the low-grade sample

shows a higher degree of liberation, the 20% TREO remaining in its tailings indicates that the rougher flotation conditions could still be further optimized.

Based on the grain size distribution, the target minerals can be classified as fine-grained. More than 85% of parisite-Ce grains across all sample grades require grinding to below 15 μm to achieve full liberation. When full liberation is achieved, the flotation rate constant is governed primarily by hydrodynamic conditions (Jameson, 2012). Pneumatic flotation cells are therefore well suited for processing such fine particles, as conventional mechanical flotation cells exhibit significant limitations in this size range (Wang and Liu, 2021). However, it is important to note that full liberation is not generally required to achieve acceptable recoveries. Nevertheless, improved liberation offers clear advantages, including an increased flotation rate constant. To better understand the effects on mineral separation, the liberation data should be interpreted in conjunction with the mineral association characteristics, as further discussed in the following section.

4.4. Mineral associations patterns and their impact on processing

Detailed characterization of mineral associations facilitates the refinement of separation strategies to achieve greater selectivity (Bradshaw, 2014). Stronger association between all REMs sub-types and ankerite in the high-grade sample compared to the other sample grades is likely attributed to the relatively greater abundance of ankerite in this material. In addition, all target REMs sub-types in the high-grade sample exhibit increased association with both ferroan dolomite and ankerite, which may influence flotation selectivity and overall recovery (Jordens et al., 2014; Nduwa-Mushidi and Anderson, 2017; Azizi and Larachi, 2018). The associations between parisite-Ce and magnetite, as well as between parisite-Ce-La and magnetite, remain consistently low in the high-grade sample. This observation aligns with the relatively low association between magnetite and REMs sub-types in both the low- and high-grade samples. It indicates greater potential for magnetite removal prior to more selective separation processes for REMs recovery from these two sample grades. Magnetic separation via LIMS and portable-Niton Xl3t X-ray fluorescence (pXRF) analyses results on the sample grades were presented in Appendix A2. Across all grades, over 90% of the TREO was recovered in the non-magnetic product. However, medium-grade sample exhibited the lowest Fe recovery and this can now be explained by the highest association of REMs sub-types with magnetite in this sample grade. Magnetic separation prior to flotation is a common technique used to remove magnetic gangue minerals, thereby creating a less complex flotation environment (Jordens et al., 2013; Yang et al., 2015; Shuai et al., 2024).

The mineral associations for parisite-Ce and parisite-Ce-La in the low- and medium-grade samples showed similar characteristics with over 60% of the associations occurring with other REMs sub-types – an indicator of relatively easier separation. Bastnäsite-Ce-La follows a similar trend, with low-grade sample having the highest association with other target mineral sub-types (over 80%), which decreases to less than 50% in the high-grade sample. Considering that bastnäsite in the low-grade sample exhibits a high degree of locking, with approximately 90% remaining locked, the association data suggest that recovery is still feasible due to its strong relation with other target minerals. For the high-grade sample, the mineral association data align well with the bastnäsite liberation results, with the former indicating 32% free surface exposure and the latter showing that approximately 65% of the grains have more than 30% of their perimeter exposed.

Among sample grades, monazite-Ce shows the lowest association with other target mineral sub-types and the highest association with apatite, which is frequently reported to occur alongside monazite (Chen et al., 2017; Nduwa-Mushidi and Anderson, 2017). It also exhibits the highest degree of association with free surface across all sample grades, consistent with the observed liberation characteristics of monazite-Ce. The strong apatite association in the medium-grade sample may influence the flotation behavior of monazite-Ce and could enable apatite recovery during the concentration stage.

Chlorite-Fe-Mg exhibits association behavior similar to that of apatite, as it also occurs alongside monazite (Overstreet, 1967; LeBoutillier and Shail, 2000; Sauber et al., 2025).

5. Conclusions

Three different sample grades from a rare earth carbonatite drill core were characterized through chemical and mineralogical analyses, which revealed significant variations in the deportment of target elements and in mineralogical composition across the samples. Different physical separation methods

were discussed, and recommendations are made based on elemental assay, modal mineralogy, liberation, and mineral association data. Each sample presents potential challenges during beneficiation. The low-grade sample, although containing a lower proportion of REMs, may still justify processing costs due to its relatively high monazite content (main host for Nd). In contrast, the medium- and high-grade samples may pose difficulties during froth flotation because of their elevated apatite and barite contents, respectively. Liberation and mineral association analyses indicate that the target REMs exhibit sufficient surface exposure to be effectively recovered by flotation at the current grind size.

In summary, the observed variations emphasize that beneficiation strategies must be tailored to each sample grade, considering the dominant REM and gangue minerals to achieve efficient and selective recovery.

Acknowledgments

This work was supported by Rare Earths Norway and EIT Raw Materials (Project No. 21130). Special thanks go to Trond Watne (Rare Earths Norway AS) for supplying the samples, Laurentius Tijhuis, Senior Engineer at IGV-NTNU, for conducting the ICP-MS analyses, and to Kjetil Eriksen, Engineer at IGV-NTNU, for preparing the polished blocks used in the SEM analysis. We are also grateful to Professor Rolf Arne Kleiv for his continued support and valuable scientific input throughout the course of this work.

References

AASLY, K., 2024. *Process mineralogy of unconventional mineral deposits: examples of applications and challenges*. Minerals Engineering, 209, 108649.

ABAKA-WOOD, G.B., QUAST, K., ZANIN, M., ADDAI-MENSAH, J., SKINNER, W., 2019. *A study of the feasibility of upgrading rare earth elements minerals from iron-oxide-silicate rich tailings using Knelson concentrator and Wilfley shaking table*. Powder Technology, 344, 897–913.

AKYILDIZ, E., SILVA, C.M., TOBICZYK, K., LODE, S., AASLY, K., KOWALCZUK, P.B., 2026. *Flotation response of parisite, monazite, bastnäsite and synchysite from a carbonatite deposit*. Powder Technology, 471, 122112.

AL-ALI, S., WALL, F., FITZPATRICK, R., BROOM-FENDLEY, S., ROLLINSON, G., BRADY, A.E., PICKLES, J.R., WILLIAMS, A., DAWES, W., 2020. *Key process mineralogy parameters for rare earth fluorcarbonate-bearing carbonatite deposits: The example of Songwe Hill, Malawi*. Minerals Engineering, 159, 106617.

ANDERSEN, T., 1984. *Secondary processes in carbonatites: Petrology of "rødberg" (hematite–calcite–dolomite carbonatite) in the Fen central complex, Telemark (South Norway)*. Lithos, 17, 227–245.

ANDERSEN, T., 1986. *Compositional variation of some rare earth minerals from the Fen complex (Telemark, SE Norway): Implications for the mobility of rare earths in a carbonatite system*. Mineralogical Magazine, 50, 503–509.

ANDERSEN, T., 1987. *A model for the evolution of hematite carbonatite, based on whole-rock major and trace element data from the Fen complex, southeast Norway*. Applied Geochemistry, 2, 163–180.

ANDERSEN, T., 1989. *Evolution of peralkaline calcite carbonatite magma in the Fen complex, southeast Norway*. Lithos, 22, 99–112.

AZIZI, D., LARACHI, F., 2018. *Surface interactions and flotation behavior of calcite, dolomite and ankerite with alkyl hydroxamic acid bearing collector and sodium silicate*. Colloids and Surfaces A, 537, 126–138.

BAGGER, A.T., KIRKELUND, G., LODE, S., JENSEN, P., KUNTHER, W., 2025. *Dissolution behavior and mineralogical changes of mine tailings subjected to NaOH solution*. Construction and Building Materials, 493, 143075.

BALARAM, V., 2019. *Rare earth elements: A review of applications, occurrence, exploration, analysis, recycling, and environmental impact*. Geoscience Frontiers, 10(4), 1285–1303.

BECKER, M., 2023. *The contribution of applied mineralogy to sustainability in the mine life cycle*. Minerals Engineering, 199, 108121.

BOESCHE, N.K., ROGASS, C., MIELKE, C., HERRMANN, S., KÖRTING, F., PAPENFUSS, A., LUBITZ, C., BRELL, M., TONN, S., ALTENBERGER, U., 2016. *Hyperspectral rare earth element mapping of three outcrops at the Fen complex, Norway: Calcitic, dolomitic, and ankeritic carbonatites*. In: DE LIMA, I.B., LEAL FILHO, W. (Eds.), Rare Earths Industry. Elsevier, pp. 235–265.

BRADSHAW, D., 2014. *The role of process mineralogy in improving the process performance of complex sulphide ores*. Keynote Paper 932, IMPC, Santiago, Chile.

BRØGGER, W.C., 1921. *Die eruptivgesteine des Kristianiagebietes. 4. Das Fengebiet in Telemark, Norwegen*. Videnskaps-Selskapets Skrifter 9, 1–402. Academy of Science, Oslo.

CAGNO, S., LIND, O.C., POPIC, J.M., SKIPPERUD, L., DE NOLF, W., NUYTS, G., VANMEERT, F., JAROSZEWICZ, J., JANSSENS, K., SALBU, B., 2020. *Micro-analytical characterization of thorium-rich aggregates from Norwegian NORM sites (Fen Complex, Telemark)*. Journal of Environmental Radioactivity, 219, 106273.

CHEN, W., HONGHUI, H., BAI, T., JIANG, S., 2017. *Geochemistry of monazite within carbonatite-related REE deposits*. Resources, 6(4), 51.

CHENG, S., LI, W., HAN, Y., SUN, Y., GAO, P., ZHANG, X., 2024. *Recent process developments in beneficiation and metallurgy of rare earths: A review*. Journal of Rare Earths, 42(4), 629–642.

DAHLGREN, S., 2019. *REE mineralization in the Fen carbonatite complex, Telemark, Norway – A world-class exploration target for the hi-tech and "green-shift" industry*. Report for the Geological Advisor, 1–86.

DAVRIS, P., MARINOS, D., BALOMENOS, E., ALEXANDRI, A., GREGOU, M., PANIAS, D., PASPALIARIS, I., 2018. *Leaching of rare earth elements from "Rödberg" ore of Fen carbonatite complex deposit using the ionic liquid HbetTf₂N*. Hydrometallurgy, 175, 20–27.

DEER, W.A., HOWIE, R.A., ZUSSMAN, J., 2013. *An introduction to the rock-forming minerals*, 3rd ed. The Mineralogical Society, London.

DROBNIAK, A., MASTALERZ, M., 2022. *Rare earth elements: A brief overview*. Indiana Journal of Earth Sciences, 4.

DRZYMALA, J., 2007. *Mineral processing: Foundations of theory and practice of minerallurgy*. Oficyna Wydawnicza PWr.

ELLIOT, H.A.L., WALL, F., CHAKHMOURADIAN, A.R., SIEGFRIED, P.R., DAHLGREN, S., WEATHERLEY, S., FINCH, A.A., MARKS, M.A.W., DOWMAN, E., DEADY, E., 2018. *Fenites associated with carbonatite complexes: A review*. Ore Geology Reviews, 93, 38–59.

ESPIRITU, E., DA SILVA, G., AZIZI, D., LARACHI, F., WATERS, K., 2018. *The effect of dissolved mineral species on bastnäsite, monazite and dolomite flotation using benzohydroxamate collector*. Colloids and Surfaces A, 539, 319–334.

EUROPEAN COMMISSION, 2023. *Study on the critical raw materials for the EU 2023: Final report*. Publications Office of the European Union.

GAJENDRA, N., YILMAZ, D., VILA, M.C., DINIS, M.L., LEVEI, E.A., TÖRÖK, A.I., AVSAR, D., KLADIS, A., PREVENIOU, A., HANSEN, A.M., AAEN, S.B., FERRANDO-CLIMENT, L., 2025. *Towards a European sustainable beneficiation of rare earth elements bearing minerals: A review*. Science of the Total Environment, 980, 179386

GEOSCIENCE AUSTRALIA, 2023. *Rare earth elements*. Geoscience Australia. Available at: webmineral.com (Accessed: 19.12.2023).

GRAMMATIKOPOULOS, T., DOWNING, S., 2020. *The disruptive role of process mineralogy in geology and mineral processing industry*. Aspects in Mining & Mineral Science, 5(2).

GRONEN, L.H., SINDERN, S., KATZMARZYK, J.L., BORMANN, U., HELLMANN, A., WOTRUBA, H., MEYER, F.M., 2019. *Mineralogical and chemical characterization of Zr–REE–Nb ores from Khalzan Buregtei (Mongolia) – Approaches to more efficient extraction of rare metals from alkaline granitoids*. Minerals, 9, 217.

GU, Y., SCHOUWSTRA, R.P., RULE, C., 2014. *The value of automated mineralogy*. Minerals Engineering, 58, 100–103.

GUNER, M.K., BULUT, G., HASSANZADEH, A., LODE, S., AASLY, K., 2023. *Automated mineralogy and diagnostic leaching studies on bulk sulfide flotation concentrate of a refractory gold ore*. Minerals, 13, 1243.

JAMES COOK UNIVERSITY, n.d. *Element-to-stoichiometric oxide conversion factors*. James Cook University.

JAMESON, G.J., 2012. *The effect of surface liberation and particle size on flotation rate constants*. Minerals Engineering, 36–38, 132–137.

JORDENS, A., CHENG, Y.P., WATERS, K.E., 2013. *A review of the beneficiation of rare earth element bearing minerals*. Minerals Engineering, 41, 97–114.

JORDENS, A., MARION, C., KUZMINA, O., WATERS, K.E., 2014. *Surface chemistry considerations in the flotation of bastnäsite*. Minerals Engineering, 66–68, 119–129.

KIM, J., CHOI, J., LEE, S., 2025. *A review of rare earth elements recovery from bastnäsite ore: From beneficiation to metallurgical processing*. Journal of Sustainable Metallurgy, 11, 773–798.

KRESTEN, P., MOROGAN, V., 1986. *Fenitization at the Fen complex, southern Norway*. Lithos, 19, 27–42.

LEBOUTILLIER, N., SHAIL, R., 2000. *The cassiterite–anatase–ilmenite–monazite–sulphide–chlorite assemblage of North Tincroft Lode*. Annual Conference of the Ussher Society.

LEJA, J., 1982. *Surface chemistry of froth flotation*. Plenum Press, New York.

LI, C., SHEN, P., ZHAO, Y., LI, P., ZHANG, L., PAN, H., 2022. *Mineral chemistry of chlorite in different geologic environments and its implications for porphyry Cu ± Au ± Mo deposits*. Ore Geology Reviews, 149, 105112.

LIE, A., ØSTERGAARD, C., 2011. *The Fen carbonatite complex, Ulefoss, South Norway. Summary of historic work and data*. 21st NORTH, Norway.

LIU, C., XU, L., DENG, J., TIAN, J., WANG, D., XUE, K., ZHANG, X., WANG, Y., FANG, J., LIU, J., 2023. *A review of flotation reagents for bastnäsite-(Ce) rare earth ore*. Advances in Colloid and Interface Science, 321, 103029.

LOTTER, N.O., 2011. *Modern process mineralogy: An integrated multi-disciplined approach to flowsheeting*. Minerals Engineering, 24(12), 1229–1237.

LOTTER, N., BAUM, W., REEVES, S., ARRUÉ, C., BRADSHAW, D., 2018. *The business value of best practice process mineralogy*. Minerals Engineering, 116, 226–238.

MALAFEEVSKIY, N., LODE, S., RØSTAD, J., LARSEN, R.B., AASLY, K., 2025. *An initial characterization for revalorization of the Joma mine tailings, Norway*. Minerals Engineering, 228, 109360.

MARION, C., LI, R., WATERS, K.E., 2020. *A review of reagents applied to rare-earth mineral flotation*. Advances in Colloid and Interface Science, 279, 102142.

MARIEN, C., DIJKSTRA, A.H., WILKINS, C., 2018. *The hydrothermal alteration of carbonatite in the Fen Complex, Norway: Mineralogy, geochemistry, and implications for rare-earth element resource formation*. Mineralogical Magazine, 82(S1), S115–S131.

MCIVOR, R.E., FINCH, J.A., 1991. *A guide to the interfacing of plant grinding and flotation operations*. Minerals Engineering, 4(1), 9–23.

NDUWA-MUSHIDI, J., ANDERSON, C.G., 2017. *Surface chemistry and flotation behaviors of monazite–apatite–ilmenite–quartz–rutile–zircon with octanohydroxamic acid*. Journal of Sustainable Metallurgy, 3, 62–72.

NKIAWETE, M.M., WAL, R.L.V., 2025. *Rare earth elements: Sector allocations and supply chain considerations*. Journal of Rare Earths, 43, 1–8.

OVERSTREET, W.C., 1967. *The geologic occurrence of monazite*. U.S. Government Printing Office, Washington, D.C.

OWENS, C.L., NASH, G.R., HADLER, K., FITZPATRICK, R.S., ANDERSON, C.G., WALL, F., 2018. *Zeta potentials of the rare earth element fluorcarbonate minerals focusing on bastnäsite and parisite*. Advances in Colloid and Interface Science, 256, 152–162.

PETRUK, W., 2000. *Applied mineralogy in the mining industry*. Elsevier, The Netherlands.

RØISI, I., AASLY, K., 2018. *The effect of graphite filler in sample preparation for automated mineralogy – A preliminary study*. Mineral Produksjon, 8, A01–A23.

SAUBER, M.E., FEO, A.D., ALMUSNED, B., HART, B., 2025. *Improved monazite flotation through combined use of oleic acid and alkyl hydroxamate: A surface chemistry approach*. Minerals Engineering, 228, 109368.

SCHULZ, B., MERKER, G., GUTZMER, J., 2019. *Automated SEM mineral liberation analysis (MLA) with generically labelled EDX spectra in the mineral processing of rare earth element ores*. Minerals, 9, 527.

SHUAI, Z., ZHU, Y., GAO, P., HAN, Y., 2024. *Rare earth elements resources and beneficiation: A review*. Minerals Engineering, 218, 109011.

SILVA, C., LODE, S., AASLY, K., KOWALCZUK, P., 2023. *Early-stage application of process mineralogy methodologies for mineral tracking in flotation of rare earth elements (REE)-bearing minerals from a deposit in Norway*. Minerals Engineering, 202, 108268.

WANG, Z.Y., FAN, H.R., ZHOU, L., YANG, K.F., SHE, H.D., 2020. *Carbonatite-related REE deposits: An overview*. Minerals, 10, 965.

WANG, D., LIU, Q., 2021. *Hydrodynamics of froth flotation and its effects on fine and ultrafine mineral particle flotation: A literature review*. Minerals Engineering, 173, 107220.

WEBMINERAL, 2025. *Webmineral database*. Available at: webmineral.com (Accessed: 05.10.2025).

WILLS, B., FINCH, J., 2016. *Wills' mineral processing technology*. Elsevier.

YANG, X., SATUR, J.V., SANEMATSU, K., LAUKKANEN, J., SAASTAMOINEN, T., 2015. *Beneficiation studies of a complex REE ore*. Minerals Engineering, 71, 55–64.

ZHANG, X., DU, H., WANG, X., MILLER, J.D., 2013. *Surface chemistry considerations in the flotation of rare-earth and other semisoluble salt minerals*. Minerals & Metallurgical Processing, 30(1), 24–37.

Appendix A1. Defined mineral recipes through detailed elemental criteria set for the main REMs subtypes

Subtype	Element	Minimum	Maximum
Parisite-Ce	La	0	38
	Ce	10	60
	Pr	0	10
	Nd	0	5
Parisite-Ce-La	La	20	45
	Ce	10	48
	Pr	0	10
	Nd	0	5
Monazite-Ce	La	0	42
	Ce	10	70
	Pr	0	10
	Nd	0	35
Bastnäsite-Ce-La	La	20	50
	Ce	32	58
	Pr	0	10
	Nd	0	12
Synchysite-Ce	La	0	2
	Ce	10	70
	Pr	0	10
	Nd	0	10

Assays of the target mineral sub-types

Mineral sub-type	Low-grade sample			Medium-grade sample			High-grade sample		
	Ce wt. %	La wt. %	Nd wt. %	Ce wt. %	La wt. %	Nd wt. %	Ce wt. %	La wt. %	Nd wt. %
Bastnäsite_Ce_La_Nd	0.002	0.001	0.001	0.004	0.003	0.002	0.028	0.020	0.011
Bastnäsite_Ce_La	0.032	0.022	0.000	0.130	0.100	0.000	0.665	0.433	0.001
Bastnäsite_La	0.003	0.000	0.000	0.000	0.001	0.000	0.000	0.002	0.000
Parisite_Ce_La	0.070	0.046	0.000	0.317	0.221	0.000	0.222	0.145	0.000
Parisite_Ce	0.060	0.008	0.000	0.171	0.028	0.000	0.190	0.038	0.000

Appendix A2. Magnetic separation results based on pXRF (tests were repeated twice under same conditions)

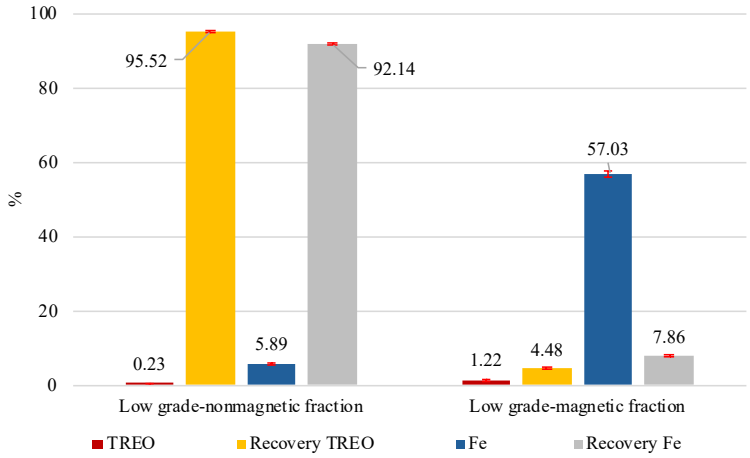

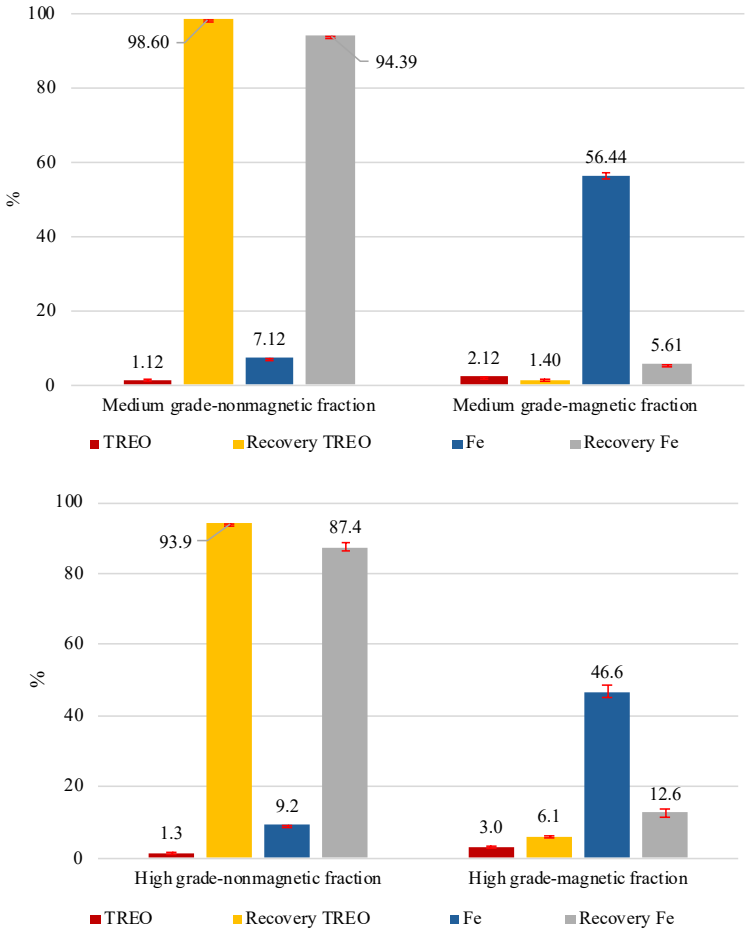

Appendix A3. Flotation results based on pXRF (tests were repeated twice under same conditions)

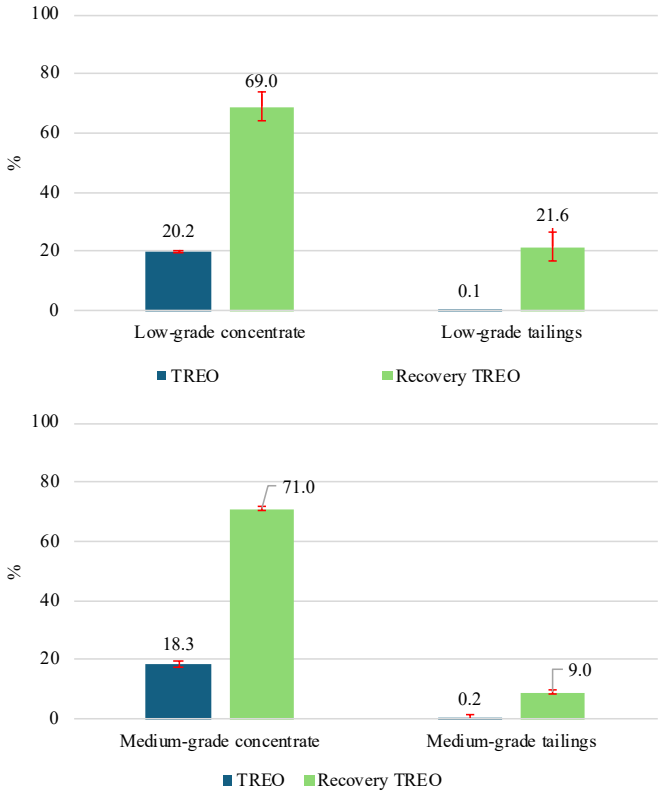

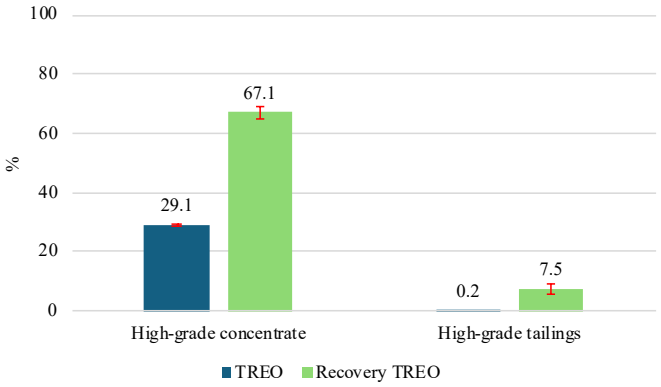
100
80
60
40
20
0
%
67.1
29.1
0.2
7.5
High-grade concentrate
High-grade tailings
TREO
Recovery TREO